CHAPTER SEVEN

The Dielectric Formalism for Inelastic Processes in High-Energy Ion–Matter Collisions

Claudia C. Montanari and Jorge E. Miraglia
Instituto de Astronomía y Física del Espacio, CONICET and Universidad de Buenos Aires, casilla de correo 67, sucursal 28, C1428EGA, Buenos Aires, Argentina

Contents

Abstract

In this chapter we analyze the possibilities and ranges of validity of the dielectric formalism to deal with correlated bound electrons in matter by using the shellwise local plasma approximation. This model describes the response of the electrons of the same binding energy as a whole (collectively), screening the interaction with the impinging ion. It considers separately each sub-shell of target electrons, with the corresponding dielectric response. The density of electrons and the energy gap are included explicitly by employing the Levine and Louie dielectric function. The goal of this chapter is to summarize and review the capability of this model to deal with fundamental magnitudes of the atomic collisions expressed as different moments of

Advances in Quantum Chemistry, Volume 65
ISSN 0065-3276, http://dx.doi.org/10.1016/B978-0-12-396455-7.00007-8

the energy loss: ionization cross sections (single or multiple, differential, and total), stopping power (and mean excitation energy), and energy loss straggling. This review covers a wide range of the collisions of ions with gases and solids, paying special attention to multi-electronic targets. The advantages and disadvantages of the model in comparison with independent electron ones, ranges of validity and future prospect will be considered.

1. INTRODUCTION

When a swift heavy particle travels through matter, different inelastic processes take place. The atomic electrons are excited or ionized, making the particle to lose energy. The probability of these events to happen, the mean energy loss during the ion passage, the effects on the target atoms (i.e., how deep are the ionized shells, what is the final charge state of the atom) are subjects of study for the different theories on heavy particle collisions.[1, 2] This research branch finds important applications in many fields, including medicine within hadron therapy (for recent reviews, see Refs. 3–6).

In this chapter we discuss the possibilities and ranges of validity of the shellwise local plasma approximation (SLPA) to deal with some of the fundamental inelastic collisions mentioned above. This is a many-electron model within the frame of the dielectric formalism, especially suitable for multi-electronic targets and high energy collisions in which target deep shells are involved.[7, 8] The SLPA describes the electronic response of each sub-shell of target electrons as a whole, including screening among electrons.[9] This is of particular interest when describing many-electron sub-shells such as $4f$ or $3d$, for example. The main characteristics of the SLPA are the independent-shell approximation (a dielectric function for each sub-shell of target electrons, meaning that only the electrons of the same binding energy respond collectively to the ion perturbation and screen among them) and the inclusion of the binding energy explicitly (not free-electron gas, but electron gas with an energy threshold).

It must be stressed that the SLPA is an *ab initio* calculation (no parameters included) whose only inputs are the atomic densities of the different sub-shells and the corresponding binding energies. It allows us to calculate the different moments of the energy loss: ionization cross sections (single or multiple, differential, and total), stopping power (and mean excitation energy), and energy loss straggling. The advantages and disadvantages of the

model, as well as ranges of validity and future prospects will be discussed in the following pages.

2. THE SHELLWISE LOCAL PLASMA APPROXIMATION

2.1 Historical aspects

When a fast heavy ion moves in a medium, it polarizes the target electron cloud. This gives rise to an induced potential, which can be described as a trailing wake that follows the motion of the projectile (see Ref. 9 and references therein). The many-body consistent treatment for an ion traveling through an homogeneous free-electron gas was developed by Lindhard[10] and by Ritchie,[11] within the linear response approximation (LRA).

This dielectric formalism was extended to deal with atomic bound electrons as a free-electron gas of local density, known as the local plasma approximation (LPA). It was applied to stopping power (energy loss per unit length) of heavy ions in matter using the logarithmic high energy limit.[12,13] Later on developments of the LPA included the extension to isolated atoms by Rosseau et al.[14] and to intermediate energies by employing the fully dielectric formulation.[15–17] In the LPA by Lindhard and subsequent works, the response of bound electrons, even local, considers the electronic cloud as a whole by using the total density of electrons in the atom.

In the last years we have improved and extended the use of the dielectric formalism to deal with bound electrons of gaseous and solid targets (insulators and metals), not only for energy loss calculations, but also for ionization probabilities and energy loss straggling.[7, 8, 18–33] The full dielectric formalism was employed together with the theoretical description of bound electrons through the atomic wave functions and binding energies.

Our developments for the SLPA had two main steps. First the separate dielectric response for each shell, by considering the independent-shell approximation. Physically, this independent-shell approximation means that when an electron of the *nl* sub-shell is ionized only the other *nl*-electrons are included in the screening of the ion potential. This gave very good results for the energy loss even at intermediate energies,[18–25] as far as the perturbative approximation is valid. A previous proposal of the independent shells within the LPA, known as the orbital OLPA, is due to Meltzer et al.[34]

However, this approach uses the logarithmic high energy limit for the stopping power.

The second step was the inclusion of the ionization gap using the Levine and Louie dielectric function.[35] This is a very important point to advance in the calculation of ionization probabilities, not only for inner-shells of metals, but also for insulators[26] and gases.[27] In this sense, the SLPA provides an interesting alternative to the independent electron models, with very good results as compared with complex formulations such as the continuum distorted wave eikonal initial state (CDW-EIS) approximation,[28] and with great advantages in the computational effort and time.

The Levine and Louie dielectric function[35] keeps the characteristics of Lindhard's,[10] i.e., electron–electron correlation to all orders, collective response, and *f*-sum rule (particle number conservation). It must be noted that the SLPA is a first order approximation (as far as the dielectric functions are calculated in LRA, like Lindhard's [10] or variations, such as Mermin's[36] or Levin–Louie's[35]). It means that it is a perturbative description valid for $Z_P/v < Z_T$ and $v > v_e$ with v_e being the mean velocity of the electrons of the *nl*-shell. The SLPA with this dielectric function proved to give good results in stopping power calculations[7, 29–33] in an extended energy range that includes the maximum of the stopping, and for inner-shell ionization of very heavy targets at high enough impact velocities.[8]

2.2 Theoretical details: The Levine–Louie dielectric function and the independent-shell approximation

Consider a bare ion of charge Z_P moving at velocity v in a free-electron gas (FEG) of homogeneous density ρ, a Fermi momentum $k^F = [3\pi^2\rho]^{-1/3}$ and a Seitz radio $r_S = [(4/3)\pi\rho]^{1/3}$. Following the dielectric formalism, the stopping power per unit length is expressed as

$$S = \frac{2Z_P^2}{\pi v^2}\int_0^\infty \frac{dk}{k}\int_0^{kv} \omega\,\mathrm{Im}\left[\frac{-1}{\varepsilon(k,\omega)}\right]d\omega, \tag{1}$$

with $\varepsilon(k,\omega)$ being the quantum dielectric function of the medium.[9] Different approximations are employed for the dielectric function, with the Mermin–Lindhard dielectric function[36] being the most accurate one to account for the plasmon time decay. This dielectric function depends on the constant density of electrons ρ and the plasmon damping γ, both characteristics obtained from the optical properties of each material[37] and from tabulations.[38]

The SLPA formulation has a general expression for the different moments of the energy loss. It describes the inelastic collision considering the interaction with each nl sub-shell of target electrons separately, with $S_{nl}^{(t)}$ being its energy moment of order t ($t = 0$ the ionization cross section, $t = 1$ the stopping power, $t = 2$ the square energy loss straggling) given by

$$S_{nl}^{(t)} = \frac{2}{\pi v^2} \int_0^\infty \frac{Z_\mathrm{P}^2 \, \mathrm{d}k}{k} \int_0^{kv} \omega^t \, \mathrm{Im}\left[\frac{-1}{\varepsilon_{nl}(k,\omega)}\right] \mathrm{d}\omega. \tag{2}$$

The total moment will be the addition of the shell contributions $S^{(t)} = \sum_{nl} S_{nl}^{(t)}$.[29] In the case of metals, electrons are treated differently depending on whether they belong to the free-electron gas (FEG) or to the inner-shells (bound electrons).

The dielectric function $\varepsilon_{nl}(k,\omega)$ in Eq. (2) is a mean value of a local response that depends on the density of electrons of the shell $\rho_{nl}(r)$ and the ionization gap ϵ_{nl}

$$\mathrm{Im}\left[\frac{-1}{\varepsilon_{nl}(k,\omega)}\right] = \int \mathrm{Im}\left[\frac{-1}{\varepsilon^{\mathrm{LL}}(k,\omega,k_{nl}^{\mathrm{F}}(r),\epsilon_{nl})}\right] \mathrm{d}r \tag{3}$$

with $k_{nl}^{\mathrm{F}}(r) = [3\pi^2 \rho_{nl}(r)]^{1/3}$ the local Fermi velocity. The dielectric function employed $\varepsilon^{\mathrm{LL}}$, is the Levine–Louie one,[35] which includes explicitly the energy gap of each shell. It is defined as

$$\mathrm{Im}\left[\varepsilon^{\mathrm{LL}}(q,\omega,k_{nl}^{\mathrm{F}}(r))\right] = \begin{cases} \mathrm{Im}\left[\varepsilon^{\mathrm{L}}(q,\omega_g,k_{nl}^{\mathrm{F}}(r))\right], & \omega > |\epsilon_{nl}| \\ 0, & \omega < |\epsilon_{nl}| \end{cases} \tag{4}$$

with $\omega_g = \sqrt{\omega^2 + \epsilon_{nl}^2}$ and $\varepsilon^{\mathrm{L}}(q,\omega,k_{nl}^{\mathrm{F}}(r))$ being the usual Lindhard dielectric function.[10] Note that if we consider no binding energy, $\epsilon_{nl} = 0$, the usual expression for the probability in the dielectric formalism (Lindhard) is recovered. Once the imaginary part is defined, the real part, $\mathrm{Re}\left[\varepsilon^{\mathrm{LL}}(q,\omega,k_{nl}^{\mathrm{F}}(r))\right]$ is obtained in closed form through the Kramers–Kronig relation, as shown in Ref. 35. This model for the dielectric function, proposed originally for semiconductors and insulators,[35] satisfies the so-called f-sum rule, or particle number conservation, that is the desirable feature for a dielectric function. In fact, this modified version of the SLPA was first applied to calculation of stopping power in insulators.[26]

The density of electrons of the shell $\rho_{nl}(r)$ and the ionization gap ϵ_{nl} are the only inputs for the SLPA. For atoms they can be obtained from the Hartree–Fock wave functions tabulated by Clementi and Roetti[39] or by Bunge et al.[40] For very heavy atoms ($Z > 54$) they can be calculated using the relativistic solutions of the Schrödinger equation.[7, 8, 32]

In the case of an ion with N bound electrons and charge state $q = Z_P - N$, the interaction with target electrons can be expressed through a screened ion-charge $Z_P^{(q)}(r)$ that depends on the distance to the nucleus (with the ion electrons frozen, just screening the nucleus). It verifies $Z_P^{(q)}(r) \to q$ for long distance collisions and $Z_P^{(q)}(r) \to Z_P$ for close collisions.

In order to include this inhomogeneous screened ion-charge in Eq. (2), instead of Z_P, we need the Fourier transform of $Z_P^{(q)}(r)$ given by

$$Z_P^{(q)}(k) = Z_P - \sum_{j=1}^{N} \left\langle \varphi_j \left| e^{i\mathbf{k}.\mathbf{r}} \right| \varphi_j \right\rangle . \tag{5}$$

Using Flannery integrals[41] and the Slater-type expansion for the projectile wave functions (Clementi and Roetti tables[39] for neutral atoms and for positive ions), $Z_P^{(q)}(k)$ has an analytical closed form (see the Appendix in Ref. 8 for the details).

We calculated $Z_P^{(q)}(r)$ for different ions from He^{+q} ($q = 0, 1$) up to Ne^{+q} ($q = 0, \ldots, 9$). In order to express it in a simple way to be included in the programs of calculus we fitted the exact $Z_P^{(q)}(r)$ with two exponentials as follows:

$$Z_P^{(q)}(r) = q + \sum_{j=1}^{2} Z_j \exp(-a_j r). \tag{6}$$

In Tables 7.1 and 7.2 we include the parameters Z_j, a_j for the different ions and charge states.

The inclusion of $Z_P^{(q)}(k)$ in Eq. (2) is straightforward. The SLPA for the total energy moment of order t due to the interaction with an ion of nucleus charge Z_P and charge state q is

$$S_{(q)}^{(t)} = \sum_{n,l} \frac{2}{\pi v^2} \int_0^\infty \frac{[Z_P^{(q)}(k)]^2 \, dk}{k} \int_0^{kv} \omega^t \, \mathrm{Im}\left[\frac{-1}{\varepsilon_{nl}(k,\omega)} \right] d\omega. \tag{7}$$

In the following sections we present and discuss the current state of the SLPA to deal with energy loss (Section 3), its straggling (Section 4), and with ionization cross sections (Section 5). The order was chosen by

Table 7.1 Parameters to fit the screened ion-charge as function of the distance to the nucleus for He^{+q} to N^{+q}. These functions were obtained using Hartree–Fock wave functions by Clementi and Roetti.[39] for neutral atoms and for positive ions

Ion	q	Z_1	a_1	Z_2	a_2
He^{+}	1	−1.289	4.722	2.289	3.529
He^{0}	0	−0.288	7.784	2.288	2.359
Li^{2+}	2	−0.101	1.017	1.101	3.411
Li^{+}	1	−0.195	0.957	2.195	3.024
Li^{0}	0	1.123	0.531	1.877	3.347
Be^{3+}	3	−0.100	1.359	1.100	4.554
Be^{2+}	2	−0.334	16.900	2.334	5.298
Be^{+}	1	1.172	0.942	1.828	4.635
Be^{0}	0	2.412	0.824	1.588	5.161
B^{4+}	4	−0.106	1.730	1.106	5.674
B^{3+}	3	3.684	7.832	−1.684	11.561
B^{2+}	2	1.250	1.376	1.750	6.138
B^{+}	1	2.532	1.255	1.468	6.823
B^{0}	0	3.631	1.075	1.369	7.285
C^{5+}	5	−0.097	2.101	1.097	6.891
C^{4+}	4	−0.208	2.120	2.208	6.459
C^{3+}	3	1.783	7.227	1.217	1.731
C^{2+}	2	2.591	1.661	1.409	8.473
C^{+}	1	3.753	1.520	1.247	9.114
C^{0}	0	4.801	1.331	1.199	9.446
N^{6+}	6	−0.058	2.353	1.058	8.420
N^{5+}	5	−0.216	2.452	2.216	7.553
N^{4+}	4	1.805	8.357	1.195	2.086
N^{3+}	3	2.639	2.077	1.361	10.093
N^{2+}	2	3.846	1.965	1.154	11.027
N^{+}	1	4.953	1.792	1.047	11.776
N^{0}	0	5.973	1.596	1.027	12.094

Table 7.2 Similar to Table 7.1 for O^+q to Ne^+q ions

Ion	*q*	Z_1	a_1	Z_2	a_2
O^{7+}	7	−0.093	2.776	1.093	9.228
O^{6+}	6	−0.207	2.825	2.207	8.744
O^{5+}	5	1.766	9.774	1.234	2.514
O^{4+}	4	1.299	10.976	2.701	2.591
O^{3+}	3	3.899	2.395	1.101	12.836
O^{2+}	2	5.043	2.237	0.957	13.962
O^{+}	1	6.113	2.052	0.887	14.782
O^{0}	0	7.087	1.824	0.913	14.749
F^{8+}	8	−0.043	2.881	1.043	11.032
F^{7+}	7	−0.130	2.543	2.130	10.157
F^{6+}	6	1.754	11.088	1.246	2.912
F^{5+}	5	1.296	13.463	2.704	2.896
F^{4+}	4	3.958	2.834	1.042	15.007
F^{3+}	3	5.190	2.750	0.810	16.145
F^{2+}	2	6.277	2.554	0.723	17.556
F^{+}	1	7.245	2.286	0.755	18.684
F^{0}	0	8.213	2.064	0.787	18.438
Ne^{9+}	9	−0.095	3.316	1.095	11.422
Ne^{8+}	8	−0.166	3.366	2.166	11.214
Ne^{7+}	7	1.787	12.100	1.213	3.247
Ne^{6+}	6	1.309	14.616	2.691	3.279
Ne^{5+}	5	1.024	16.471	3.976	3.256
Ne^{4+}	4	5.181	3.129	0.819	19.045
Ne^{3+}	3	6.299	2.953	0.701	21.086
Ne^{2+}	2	7.350	2.738	0.650	22.470
Ne^{+}	1	8.360	2.524	0.640	23.075
Ne^{0}	0	9.326	2.306	0.674	22.586

historical reasons: the dielectric formalism, and more specifically, the local plasma approximation, was developed to describe the energy loss of heavy particles in solids. Instead, using a collective formalism to calculate ionization probabilities of solids and, even more of gaseous targets, is much more demanding and is new theoretical development due to the SLPA.

3. ENERGY LOSS IN PARTICLE PENETRATION OF MATTER

The mean value of the energy loss of particles in matter, also known as stopping power, is a necessary ingredient of many parts of basic science, of medical and technological applications.[42, 43] It is an average of the ion energy loss per unit path length. At intermediate to high impact velocities, this energy loss is related to ionization of target electrons. The higher the ion energy, the deeper the excited electrons. In the case of metals, it means that at intermediate and high impact energies, the description of the stopping power due to excitation of valence electrons (the FEG of metals) is not enough, and target inner-shells must be included.

Different experimental methods are used to determine stopping powers[44] and important collections of data, statistics, and semiempirical functions are available in the web.[45, 46] Many semiempirical and theoretical models have been developed (see Refs. 47–50 and references therein). However, the description of very heavy targets, i.e., those with the close 4*f* sub-shell with 14 electrons, remains a heavy task for first principle theoretical calculations. On the contrary, the SLPA, being a many-electron model, describes with the same degree of complexity Ne, Cu, or Au targets. Furthermore, the more electrons the shell has, the more suitable the method is. On the other hand, this model works within the dielectric formalism, so dynamical screening effects among electrons are included. This proved to be of particular interest for the case of the *f*-shells.[32]

The only inputs for the SLPA are the density of electrons around the nucleus for each sub-shell and the binding energy. As far as these inputs are known, the SLPA calculations reduce to rather simple numerical integrations, given by Eqs. (2) and (7). Moreover, the extension of this formalism to deal with complex targets (compounds, molecules of biological interest, water) is straightforward if these inputs are known.

3.1 The SLPA in stopping power of metals for protons

The SLPA gives good results for energy loss by protons in metal targets.[7, 31, 32] We consider and discuss here three cases of special interest , Cu ($Z=29$), W ($Z=74$), and Au ($Z=79$). This choice is founded on their experimental

and technological interest, and on the availability of data. Cu and Au are the two targets with the largest amounts of stopping measurements. For W, new interest is related to its properties as inner-wall of fusion reactors.[51] For our theoretical interest, these are targets for which outer electrons can be described as FEG and we can deal separately with bound electrons using the SLPA. This separate description of the response of bound and valence electrons as inhomogeneous and homogeneous electron gases, respectively, is part of the good agreement obtained. On the other hand, the separate calculations allow using different models in each case (i.e., the SLPA for bound electrons and a non-perturbative formalism for the FEG).

For Cu, the densities and binding energies were obtained from the tabulated Hartree–Fock wave functions.[39, 40] For Au and W, the atomic wave functions are the solutions of the relativistic Dirac equation instead the nonrelativistic Schrödinger equation. We employed to this end the fully relativistic *ab initio* wave functions obtained by using the HULLAC[52] code (see Ref. 7 for the details). The binding energies were compared with tabulated experimental binding energies in solids by Williams.[53]

For H ions in solids we calculate the stopping cross section just considering H^+ (Refs. 7, 32). At low velocities, the screening of the H^+ nucleus is strong enough to have very loose or directly no bound electron.[54, 55]

The total stopping of protons in Cu is displayed in Figure 7.1. This value was obtained by adding the bound electron and the FEG contributions. The former was calculated with the SLPA formalism (Eq. (2) with $t = 1$) and adding the contributions of the different sub-shells to get total stopping of bound electrons. The latter by employing the dielectric formalism (perturbative approximation) with the Mermin–Lindhard dielectric function.[36] The characteristic plasmon frequency and width employed here for Cu FEG are $\omega_p = 0.703$ a.u. and $\gamma = 0.950$ a.u., respectively. This yields a mean value of electrons in the FEG as $N_e = 3.14$, and a Seitz radius as $r_S = 1.82$ a.u. These values were obtained from the optical data of the energy loss function[37] by considering only the first important peak. These number of electrons in the FEG is similar to the experimental value recommended by Isaacson.[38] To keep the total number of electrons, we considered Cu as [Ar] $3d^{7.86}$ and the "3.14" electrons as FEG.

In Figure 7.1 we compare our total stopping cross sections of Cu for protons, with the experimental data available,[45] and with SRIM08 results.[46] The contribution from the FEG and the bound electrons are

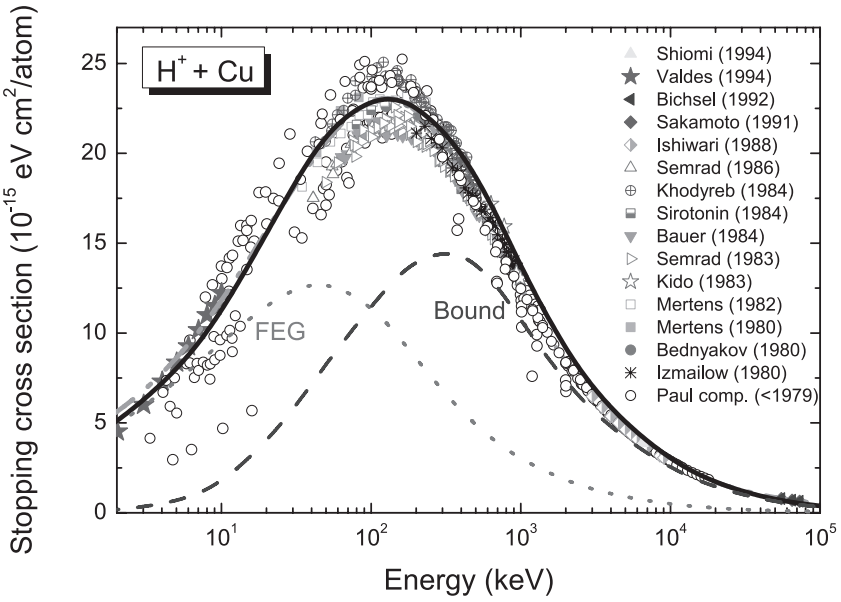

Figure 7.1 Stopping cross sections of Cu for protons. Curves: solid line, total stopping adding the contributions by bound electrons (blue dashed line, SLPA) and by the FEG (red dotted line, Mermin–Lindhard dielectric calculation); orange dash dotted line, SRIM08 results.[46] Symbols: experiments as reported by Paul;[45] different symbols marked within the figure, experimental data since 1980; black hollow circles, experimental data corresponding to (1935–1979).

displayed separately. About the experimental data, we indicate separately only the data since 1980, while earlier data is plotted together with a single type of symbol. The agreement with the experimental data and with the SRIM08 curve[46] is very good in the whole energy range. The stopping maximum is correctly described in energy and value. The differential description for the FEG and the bound electron contribution is the basis for this agreement.[56]

We display in Figures 7.2 and 7.3 the stopping cross sections of Au and W for protons.[7, 32] These are very interesting targets because the $4f$ sub-shell plays a major role. For solid Au, we describe the FEG with the Mermin–Lindhard dielectric function and the following parameters (in atomic units): Seitz radio $r_S = 1.17$ a.u. (17 electrons in the FEG), plasmon energy $\omega_P = 1.37$ a.u., and a damping $\gamma = 1.37$ a.u. These values were obtained as a first approximation to optical energy loss function tabulated in the Handbook of Optical Constants by Palik and Ghosh.[37] This means that the atomic $5p^6$, $5d^{10}$ and $6s^1$ electrons are considered as the homogeneous FEG, and the first bound electrons are those of the $4f$ sub-shell. The bound electron contribution was calculated using the SLPA with the fully relativistic wave functions and binding energies.[7]

In Figure 7.2 we display our theoretical results for the stopping cross section together with the large amount of experimental data available,[45] and the SRIM 2008 values. The contributions of the FEG and the bound electrons are displayed separately. The FEG contribution in gold, even the main one, cannot explain the total results for energies above 100 keV. As observed in the figure, there is an important dispersion of experimental values, mainly around the stopping maximum, which makes any theoretical description not conclusive. In order to have a cleaner picture of the situation, we displayed separately the stopping measurements of the last 25 years. This arbitrary classification allowed us to note that, except for the results by Martinez-Tamayo et al.[57] the latest stopping measurements tend to be close to a single curve. The semiempirical SRIM08 code [46] gives a curve in accordance with these latest experimental data.

The total stopping cross section obtained using the SLPA for bound electrons describes well the experimental data in the whole energy range. It has a maximum at 130 keV, shifted and higher than SRIM08,[46] and in rather good agreement with theoretical predictions by Heredia-Avalos et al.[58] and

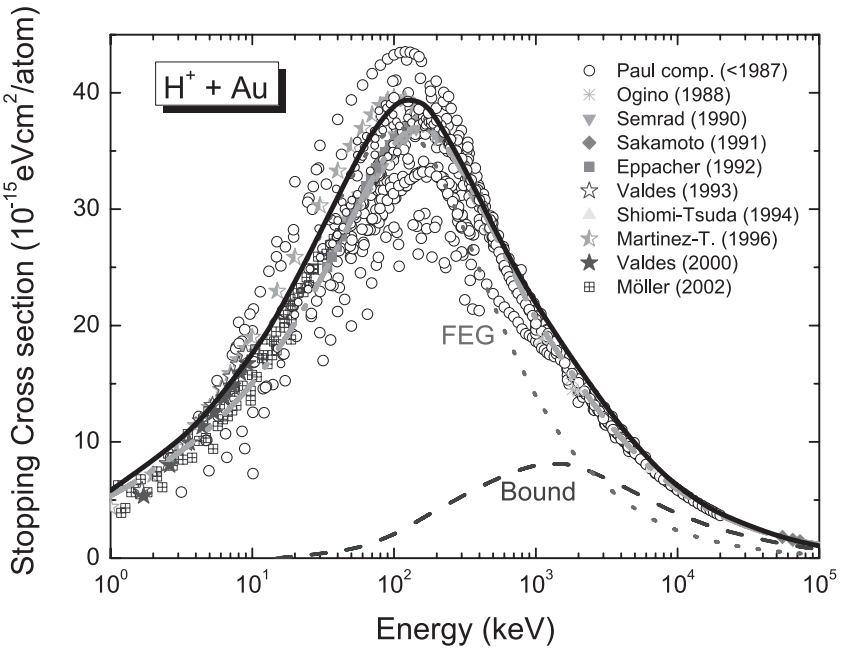

Figure 7.2 Stopping cross section of Au for protons. Curves: dashed line, present SLPA calculation for the bound electrons; dotted line, FEG contribution using the Mermin–Lindhard dielectric function;[36] solid line, total stopping as the addition of the previous two contributions; dashed dotted line, SRIM08.[46] Symbols: experiments as reported by Paul;[45] different symbols within the figure are data since 1987; hollow circles, previous measurements.

with the measurements by Martinez-Tamayo et al.[57] and to previous ones by Kreussler et al.[59] and Santry and Werner.[60]

It is worth mentioning that the relativistic results for the binding energies of Au show spin-orbit split in energy $E_{n,l,l\pm\frac{1}{2}}$ (see Fig. 1 in Ref. 7). It is an important point, because these are sub-shells that are very close in energy. As mentioned before, the SLPA describes collectively those electrons with *equal* binding energy, allowing screening among them. We use $E_i \pm \Delta E_i$ as criterion of *equal* binding energy, with ΔE_i being the quantum uncertainty

$$\Delta E_i \approx \frac{1}{\Delta t_i} = \frac{v}{\langle r \rangle_i}, \tag{8}$$

with E_i and $\langle r \rangle_i$ being the energies and mean radius of the sub-shell.

Using this criterion we have found that in the cases studied, the spin-orbit split is not resolved. Physically this implies that the 14 electrons of the $4f$ sub-shell respond together shielding the projectile, and not the 8 electrons $4f_{7/2}$ and the 6 electrons $4f_{5/2}$ separately. This separated or not-separated response of the sub-shells is very clear in the case of protons in W, as displayed in Figure 7.3. For W, not only cannot the $4f_{7/2}$ and $4f_{5/2}$ be resolved, but there is also inter-shell screening between $5p$ and $4f$ electrons. As displayed in Table 7.3, these sub-shells are very close in energy and respond collectively to the ion passage. The importance of this effect is clear

Table 7.3 Fully-relativistic binding energies of the N and O-shells of Au and W. These results have been calculated by Mitnik and collaborators[7, 32] with the HULLAC code[52] for isolated atom. Also included are the experimental values, E^{expt}, compiled by Williams.[53] The binding energies are in atomic units

	$E^{\text{expt}}_{\text{Au}}$	$E^{\text{th}}_{\text{Au}}$	$E^{\text{expt}}_{\text{W}}$	E^{th}_{W}
$4s$	28.0	26.0	21.8	20.8
$4p_{1/2}$	23.6	22.8	18.0	17.3
$4p_{3/2}$	20.1	19.2	15.6	14.8
$4d_{3/2}$	13.0	12.5	9.40	9.0
$4d_{5/2}$	12.3	11.9	8.95	8.5
$5s$	3.94	4.1	2.78	2.9
$4f_{5/2}$	3.22	3.2	1.23	1.3
$4f_{7/2}$	3.08	3.1	1.16	1.2
$5p_{1/2}$			1.66	1.9
$5p_{3/2}$			1.35	1.5

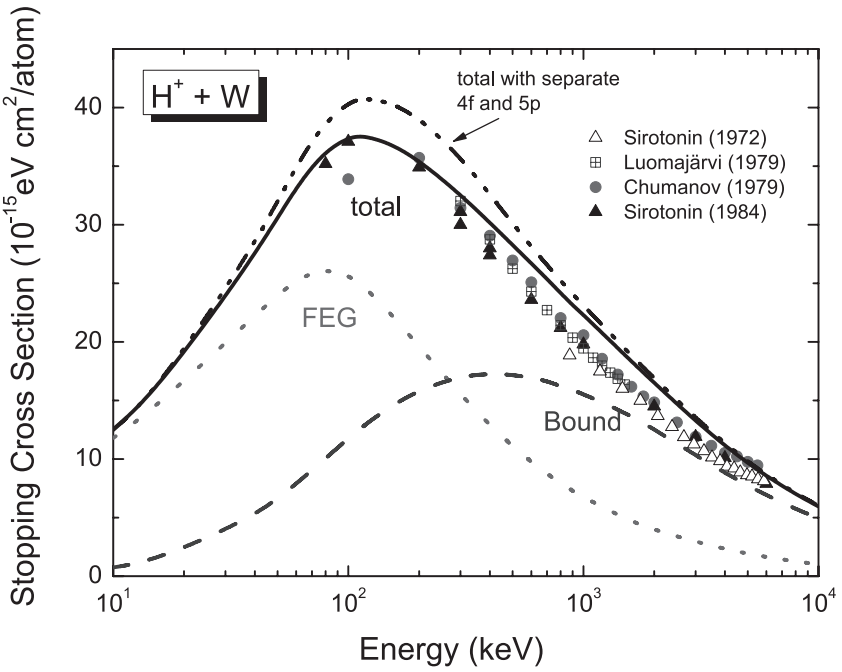

Figure 7.3 Stopping cross sections of W for protons. Curves: solid lines, present theoretical results for the contributions by bound electrons (SLPA) and the FEG, and total stopping as the addition of the previous two; dash lines, results obtained using the SLPA with independent $5p$ and $4f$ responses. Symbols: different symbols within the figure are the experimental data as reported by Paul.[45]

while comparing total theoretical and experimental stopping in Figure 7.3. Note that the screening among electrons reduces the stopping cross section in all the cases (in Au, too). This effect can only be taken into account with a many-electron model and a collective description of bound electrons. The results displayed in Figure 7.3 describe the stopping maximum quite well. However an overestimation of the experimental data around 2 MeV is found. We will return to this matter in the following section in relation to the Bethe high energy limit.[61]

3.2 Stopping number and Bethe limit

The SLPA provides an interesting alternative to describe the energy loss of different materials for energetic ions. At high energies the ion losses energy due to the interaction with deep bound electrons, so the behavior of the stopping power at high energies is a good test for the model.

The stopping power can be expressed in terms of the dimensionless stopping number $L(v)$ as

$$S(v) = \frac{4\pi Z_P^2 Z_T}{v^2} L(v). \tag{9}$$

In the high-but-nonrelativistic velocity regime, the stopping number is described by the Bethe asymptotic formulae[61]

$$\lim_{v\to\infty} L(v) = L^{\text{Bethe}}(v) = \ln\left(\frac{2v^2}{I}\right), \tag{10}$$

with I being the mean excitation energy, characteristic of each target.[62] Our theoretical description of the energy loss should converge to the Bethe high (but nonrelativistic) energy limit.

In Figure 7.4 we display the stopping number comparing the SLPA, Bethe limit, and SRIM08 values,[46] the latter representing the behavior of the experimental data for each target. Using the Lindhard and Scharff scaling with v^2/Z_T (valid for elements of high atomic number[63]) we plot together the SLPA results for the stopping number of W and Au. The straight-line in the logarithmic scale of v^2 is the Bethe limit.

It is an interesting figure because different aspects can be observed: the Lindhard and Scharff scaling is valid for W and Au; the SLPA tends to the Bethe limit, as expected theoretically; the description of the experimental data with the SLPA is good at the lower energies displayed in this figure, but in the high energy region the SLPA is closer to Bethe than to the experiments. This is a 10% of theoretical-experimental difference in the energy region 1–4 MeV, the energy region observed in Figure 7.3.

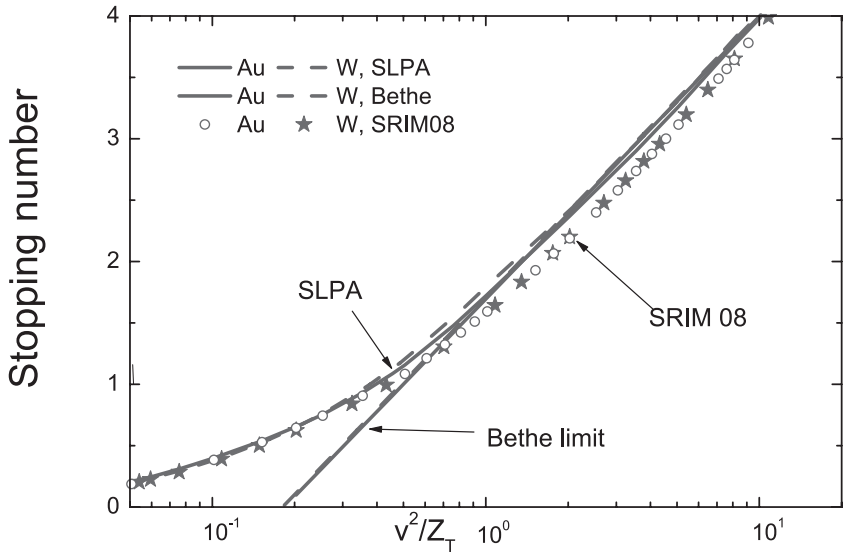

Figure 7.4 Lindhard scaling for the stopping number L. Curves: SLPA results for Au (solid line) and W (dashed line); Bethe high energy limit obtained using Eq. (10) and the mean excitation energies I suggested by the ICRU49 Report (Ref. 44) $I_W = 727 \pm 30$ eV, and $I_A u = 790 \pm 30$ eV. Symbols: SRIM08 values for Au (hollow circles) and W (stars).

This means a certain overestimation by the SLPA in the high energy region, which is related to the theoretical tie to the Bethe limit.

3.3 Stopping for dressed ions

By dressed ions we mean those ions with bound electrons, whether they be neutral or with a certain charge state. In this case, while the ion moves through a medium, loss and capture processes take place until reaching an equilibrium distribution of charge states q ($q = 0, \ldots, Z_P$) within the foil, depending on the ion velocity v. In the equilibrium regime, the mean energy loss will be the average of the stopping cross sections $S_{(q)}$ given by Eq. (7), with the calculated screened ion-charge (Tables 7.1 and 7.2), weighted with the data of fraction of ions with charge q at that velocity, $\phi_q(v)$. Namely

$$S = \sum_{q=0}^{Z_P} \phi_q(v) S_{(q)}. \tag{11}$$

The equilibrium charge fractions at each impact velocity, $\phi_q(v)$, are external inputs. A fitting of a large amount of experimental values of charge states exiting the solid, combining different ions and targets is due to Schiwietz and Grande.[64] It is available within the CasP5.0 code.[65]

On the other hand, for ions with nuclear charge $Z_P \geqslant 2$, the perturbative description for the FEG contribution is found to underestimate the experimental data for energies below that of the maximum of stopping power. For this reason for He and heavier ions we combine the SLPA for the bound electrons with a non-perturbative model for the FEG. As the energy loss by ionization of inner-shells contributes at high energies, the perturbative approximation used in the SLPA is still valid. In fact, for the stopping power of Zn for different ions we found the description of bound electrons ($1s$ up to $3d^9$) with the SLPA to be valid for He up to C projectiles, as displayed in Figure 7.5. For O ions in Zn the perturbative SLPA overestimates the total stopping cross section.[33]

Figure 7.5 summarizes previous results for the different ions[22, 29, 30, 33] in Zn. The non-perturbative model for the FEG employed in these calculations is the Transport Cross Section-Extended Friedel Sum Rule (TCS-EFSR) approach by Arista and coworkers.[66, 67]

To analyze in detail the stopping of dressed ions in matter, we consider the stopping of Cu and Au targets for He. In Figure 7.6 we display the

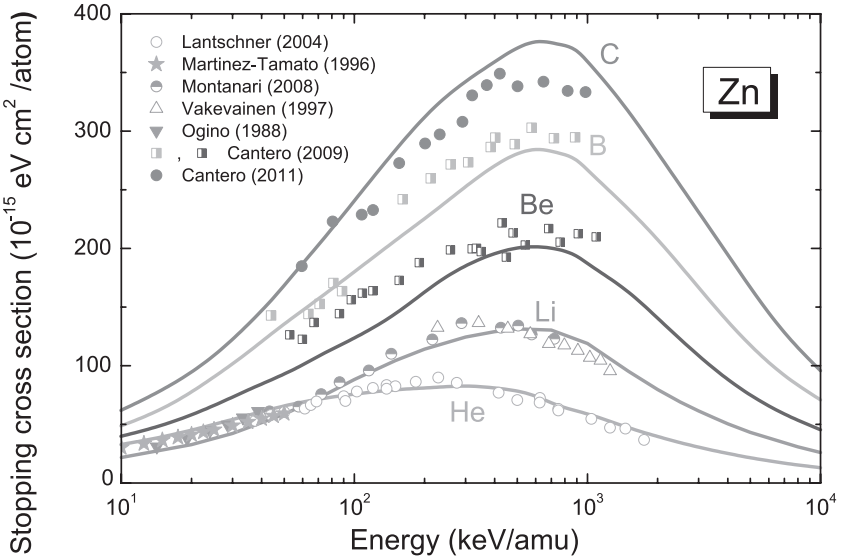

Figure 7.5 Total stopping cross sections of different ions in Zn. Curves: theoretical calculations adding SLPA for bound electrons and HISTOP (non-perturbative) for the FEG.[22, 29, 30, 33] Symbols: experimental data for He, Li, Be, and B ions as in Figure 6 of Cantero et al.;[30] for C ions, Cantero et al.[33]

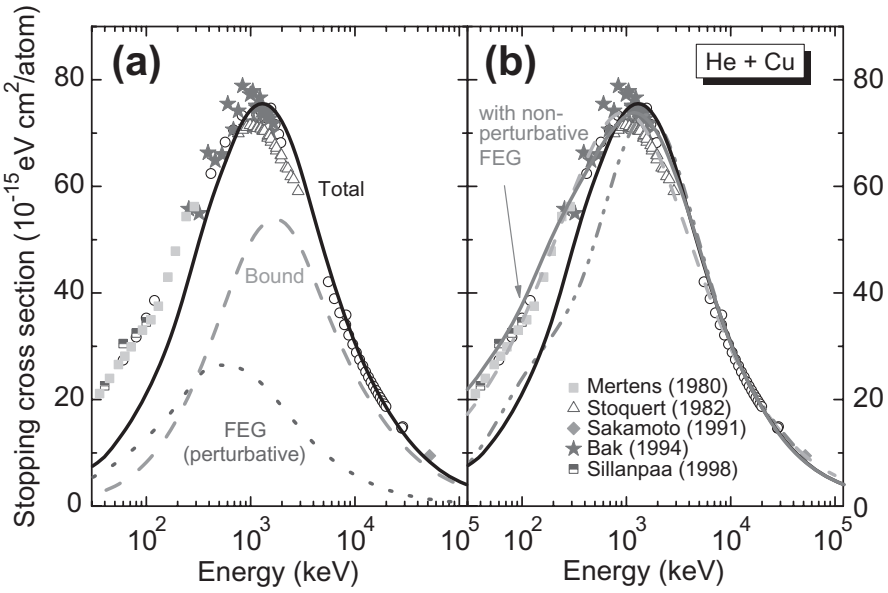

Figure 7.6 Stopping cross sections of Cu for He ions. Curves: (a) dashed line, the bound electron contribution obtained using the SLPA; dotted line, the FEG contribution with Mermin dielectric function (perturbative); solid line, total stopping adding both contributions (similar to Figure 7.1); (b) black solid line, total stopping adding the SLPA results for bound electrons and a perturbative description for the FEG with Mermin dielectric function as in (a); gray solid line, total stopping adding the SLPA results for bound electrons and a non-perturbative model for the FEG by Arista for He in Zn;[22] dashed dotted line, SRIM08;[46] dashed double-dotted line, Casp5.0.[65] Symbols: experiments as reported by Paul;[45] different symbols within the figure are data since 1980; hollow circles, previous measurements.

partial and total stopping cross section for He in Cu. In Figure 7.6a the contributions of bound electrons and FEG are displayed separately. The former calculated with the SLPA, the latter with the dielectric formalism (perturbative, LRA), using the Mermin–Lindhard dielectric function (similar to the case of protons in Cu). The behavior of the total stopping displayed in Figure 7.6a has already been found for Zn (Ref. 22), i.e., below 100 keV/amu ($v < 2$ a.u.) the perturbative model does not describe the experimental data. The replacement of the perturbative FEG-stopping by the non-perturbative one gives the total stopping displayed in Figure 7.6b. For the FEG we employed, as first approximation, the results for the FEG of Zn for He (with $r_s = 2.02$) by Arista using the TCS-EFSR in Ref. 22. The theoretical-experimental disagreement at low energies may be related to this. However, the tendency to correct the underestimation due to the perturbative calculation is clear. We also include in Figure 7.6b Schiwietz and Grande results with the unitary convolution approximation (UCA) for swift particles (available in the CasP5.0 code[65]), and the semiempirical values by the SRIM08 code.[46] Above the stopping maximum all the theoretical results agree quite well. For energies below this value the combination of different calculations, for bound electrons and FEG shows very good agreement if the non-perturbative FEG model is used.

For He in Au, in Figure 7.7 we display the theoretical results obtained in perturbative approximation, with the SLPA for bound electrons and Mermin–Lindhard dielectric function for valence electrons. As observed in the case of protons in Au, for He in Au the dispersion of the experimental data is important for impact energies below the stopping maximum. The theoretical description is quite good for impact energies above 400 keV. The maximum of the stopping is correctly described around 1 MeV. For energies below 400 keV we are outside the limit of validity of the perturbative approximation. The combination of SLPA with a non-perturbative description for stopping due to valence electrons of Au (as for Cu or Zn targets) is expected to improve these results.

4. ENERGY LOSS STRAGGLING

The theoretical square energy loss straggling, Ω^2, or the second moment of the energy loss ($t = 2$ in Eqs. (1) and (7)), describes the statistical dispersion of the energy loss. It represents the energy loss variance per unit path length of a Gaussian-type energy loss distribution.[68] The condition for obtaining a Gaussian distribution is that the energies transferred in

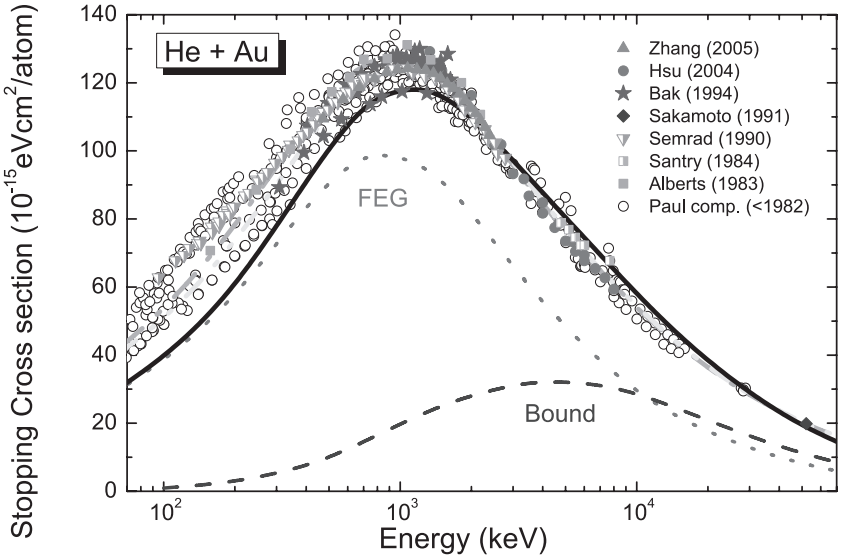

Figure 7.7 Stopping cross sections of Au for helium. Curves: dashed line, the bound electron contribution obtained using the SLPA; dotted line, the FEG contribution with Mermin dielectric function (perturbative); solid line, total stopping adding both contributions (similar to Figure 7.1); dashed double-dotted line, SRIM08 results;[46] dashed dotted line, ICRU49;[44] dashed double-dotted line, Casp5.0.[65] Symbols: experiments as reported by Paul;[45] different symbols within the figure are data since 1982; hollow circles, previous measurements.

the individual collisions should be small as compared to the width of the final distribution.[69]

The high energy limit for the energy loss straggling was calculated by Bohr[69] as

$$\Omega_{\mathrm{B}}^2 = 4\pi Z_{\mathrm{P}}^2 Z_{\mathrm{T}}, \tag{12}$$

which is proportional to Z_{T}, the total number of target electrons active in the collision at sufficiently high energies.

The energy loss straggling is an interesting parameter to study theoretically and experimentally. It represents a sensitive input for many calculations (Ziegler[46] or Ma et al.[70]) and computer simulations, like SIMNRA by Mayer[71] for material analysis, or SEICS by Garcia-Molina and coworkers[72, 73] for elements of biological interest.

For the stopping power, there are important compilations of data available[45] and wellknown and tested semiempirical programs[46] and recommended values.[44] However, the situation is completely different for energy loss straggling. The most widely used electronic energy loss straggling is Yang empirical fitting[74] included in modern ion beam analysis codes such as SIMNRA, NDF, CORTEO, and MCERD.[75] However the accuracy of this formulae is questioned

for different reasons.[25, 76] The source of the Yang expression is a compilation of data prior to 1990 which presents serious problems. Measurements of energy loss straggling set severe requirements to target preparation (well defined thin films, uniformity, and homogeneity).[77] Experimental methods, such as transmission or Rutherford back scattering, are very sensitive to roughness and inhomogeneity of the samples, which introduce important additional energy loss straggling, especially at low energies.[68,77,78] It produces overestimation in a region around the stopping maximum[68] and an important dispersion among data. The weight of this contribution in the experimental straggling is clear in some measurements previous to 1980 included in Yang''s compilation and fitting.[74] Fortunately, there is a great number of recent measurements from different laboratories and using different techniques that show less spread and tend to be close to a single band.[79–85]

In this section we present different theoretical results calculated with the SLPA. These results improve those by Chu[86] using the LPA with Hartree–Fock densities and considering the electronic cloud as a whole. The difference between our results and those by Chu is the shell to shell description of the dielectric response.

In Figure 7.8 we display the SLPA results for square energy loss straggling normalized to Bohr value[69] for H and He ions in Cu. The different

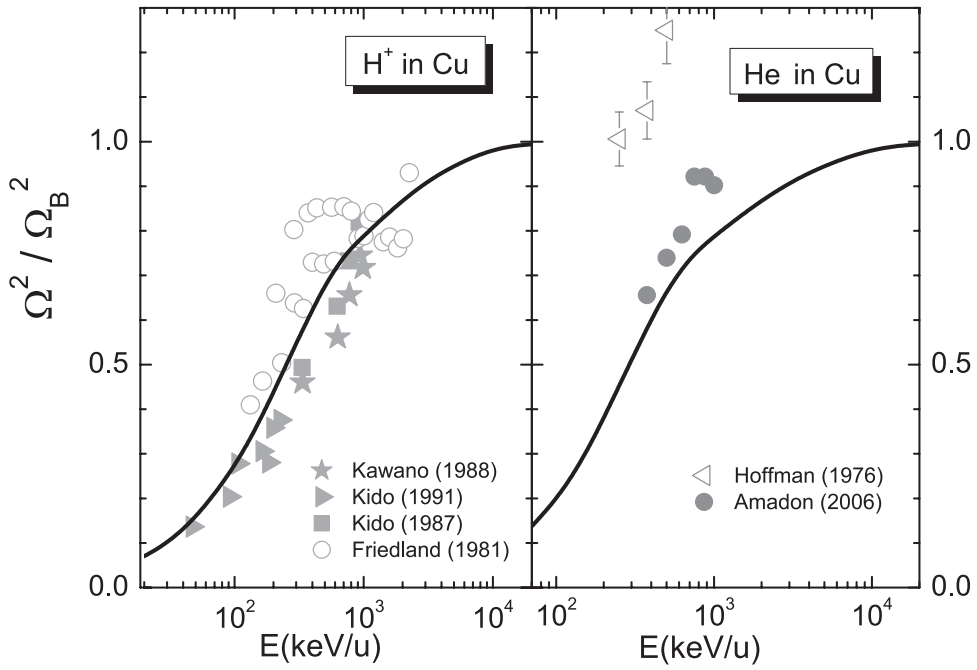

Figure 7.8 Squared straggling of Cu for H and He ions, normalized to Bohr high energy limit. Curves: solid lines, our SLPA results. Symbols: experimental data as indicated in the figure. For H^+ in Cu (Refs. 80–82, 88); for He in Cu (Refs. 83, 87).

charge states of He in Cu were considered to obtain these values, however no important differences with respect to He^{2+} were obtained for energies above 200 keV/amu. We include in Figure 7.8 the experimental data by Hoffman and Powers[87] and by Friedland and Kotze,[88] which are not corrected to exclude the inhomogeneity contribution. The overshooting of these values is clear, mainly in the data by Hoffman and Powers.[87]

The SLPA values for the energy loss straggling tend to the Bohr limit from below, and do not show the overshooting (Bethe–Livingston shoulder[89]) around the energy of maximum stopping power predicted by the binary collision formalisms.[89, 90] At high energies, the square energy loss straggling tends to a value proportional to the total number of target electrons, as predicted by Bohr.[69] If we calculate the square straggling as

$$\Omega^2/\Omega_B^2 = \sum_{nl} \Omega_{nl}^2/\Omega_B^2, \tag{13}$$

we can say that each term verifies that $\Omega_{nl}^2/\Omega_B^2 \rightarrow N_{nl}/Z_T$, with N_{nl} being the number of electrons in the nl sub-shell.[7, 25] This is an interesting point because it indicates the high energy limit expected for each shell. But it also represents a demanding requirement for the theoretical calculation, because all shells, even deep ones, contribute to the total straggling, i.e., the L-shell of Au with eight electrons is 10% of the Au energy loss straggling.

On the other hand, we found that the energy loss straggling normalized to Z_P^2 (Bohr limit) is almost independent of the ion atomic number Z_P, at least for low Z ions showing a perturbative dependence with the ion-charge.[25] In order to test this in Figure 7.9 we plotted together the experimental data for different ions in Au together with the SLPA values for the bare ions in Au. The experimental data included are those that explicitly take into account the roughness and inhomogeneity of the sample. In the case of the experimental data by Andersen et al.[91] they have been corrected in 10% due to the estimation of this contribution. The data by Møller et al. shows asymmetric error bars that correspond to Figure 5 in Ref. 92.

We can observe that the soft dependence with the ion-charge of the experimental data normalized to Bohr limit is valid at least for H, He, and Li ions. The data for B in Au by Hsu et al.[79] could indicate a deviation for higher Z ions. On the other hand, Figure 7.9 emphasizes the good description of the straggling obtained with the SLPA, even for unexpected low energies. Note that all target electrons have been considered in the calculation, even the very deep ones.

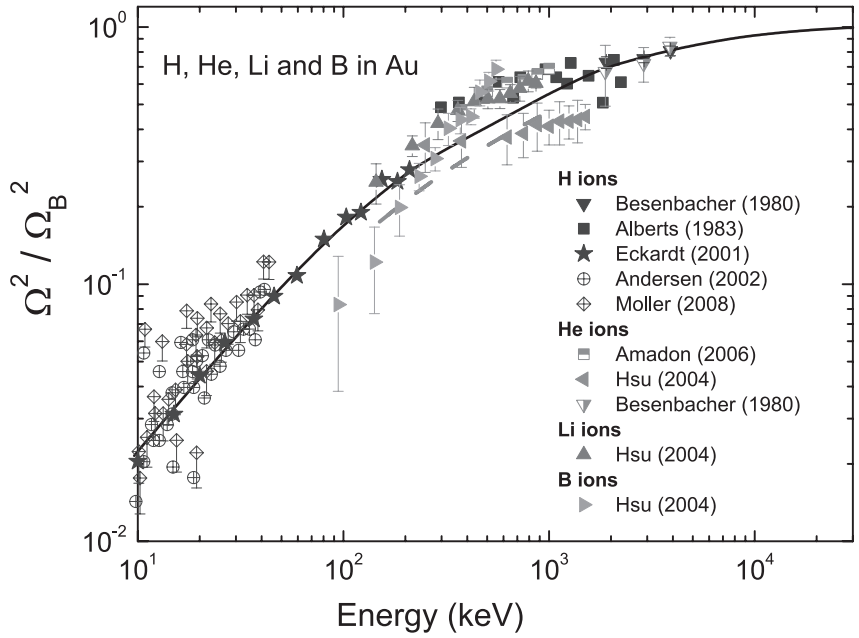

Figure 7.9 Squared straggling of Au for H, He, Li and B ions, normalized to Bohr high energy limit. Curves: solid line, SLPA straggling for bare ions; dashed line, Chu values.[86] Symbols: indicated in the figure; for H ions;[68, 84, 85, 91, 92] for He ions;[68, 79, 83] for Li and B ions.[79]

Based on the interest in new general expressions for the energy loss straggling, we used Lindhard's scaling, which proved to be valid for stopping by high Z-targets. In Figure 7.10 we plotted the square energy loss straggling normalized to Bohr, as function of v^2/Z_T, including experimental data for different ions (H to B) and targets (Cu, Au, Pb, and Bi). The theoretical SLPA results for Au to Bi are actually very close (they are hardly distinguishable in this figure). The SLPA results for Cu (dashed line) separates slightly from the others. This scaling for the energy loss straggling is an interesting proposal because it introduces the possibility of a simple universal function to describe it.

4.1 The SLPA for stopping and straggling of gases

The SLPA evolved from models developed to deal with solid targets. However there is no reason to restrict its use just to solid targets. The response of bound electrons employed is based on the atomic wave functions and binding energies, described in full Hartree–Fock or Hartree–Fock–Dirac methods (the latter for targets with $Z_T > 54$) .

In the previous sections we show the performance of the SLPA, with good results for the description of the energy loss of ions in solid matter, is

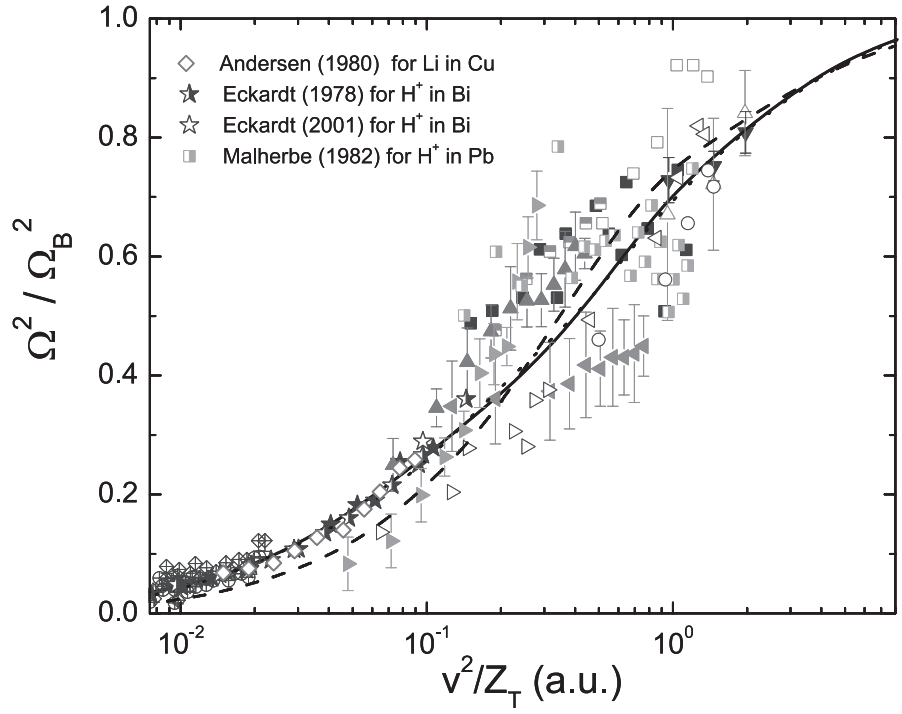

Figure 7.10 Scaling for the squared straggling normalized to Bohr as function of Lindhard parameter v^2/Z_T. Curves: SLPA results for Au (solid line), Bi (dotted line) and Cu (dashed line). Symbols: similar to Figures 7.8 for H and He in Cu and to 7.9 for different ions in Au; additional data included[84, 93–95] as signed inside the figure.

the intermediate to high energy region. In Figures 7.11 and 7.12 we display the SLPA results for stopping and straggling of protons in four rare gases, and compare them with experimental data available.

Note that for gaseous targets we should include not only the ionization channel (as for solid Cu or Au, for which the valence electrons as FEG fills the outer bands). For gases, the excitation channel is allowed. For the rare gases we use the SLPA formulation given by Eq. (2) with energy gaps equal to that to the first excited state (i.e., in atomic units, we use for Ne, $E_{3s} = -0.1809$; for Ar, $E_{4s} = -0.1666$; for Kr, $E_{5s} = -0.1598$; for Xe, $E_{6s} = -0.1517$). The energy gap is a sensitive point in the SLPA. Different values for these excitation energies will change present results.

We display in Figures 7.11 and 7.12 the SLPA stopping and straggling of rare gases for protons. The stopping description in Figure 7.11 is good for proton impact above 300 keV in all the rare gases. Below this energy the theoretical values underestimate the data, especially for Ar. These results look quite different from those in metals. This is not surprising. In general stopping power in metals is better known and described than in gases. For example, for stopping of Ne, Ar, and Kr the very recent calculations by

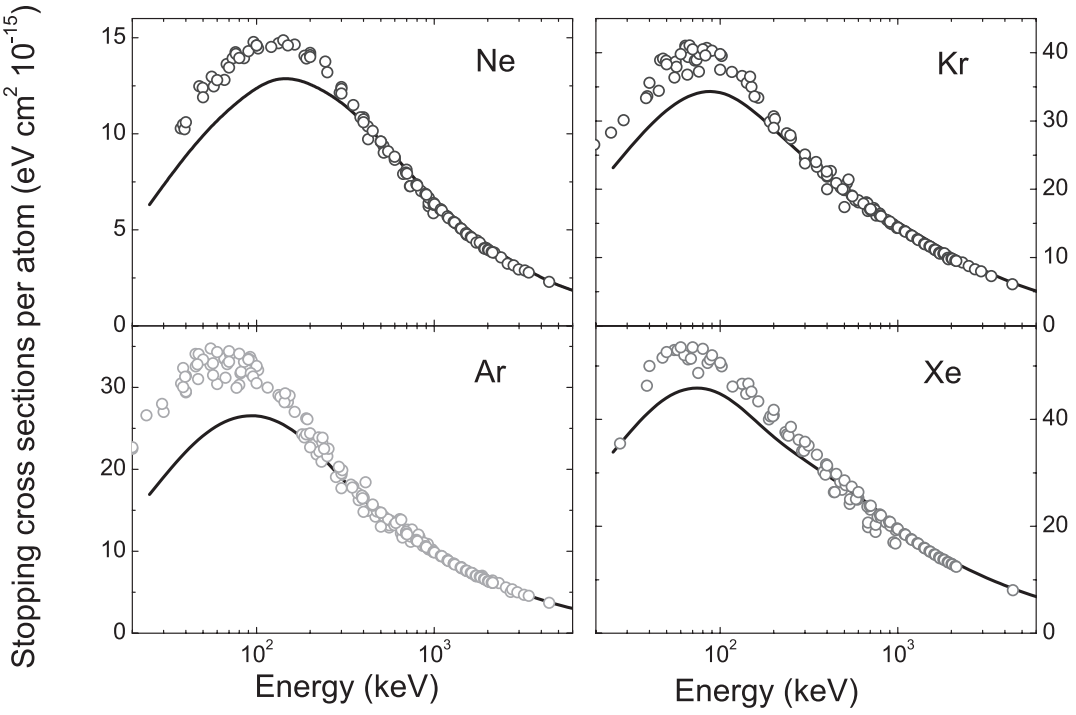

Figure 7.11 Stopping cross section of rare gases for H^+. The curves correspond to the SLPA results. The experimental data is available in Ref. 46.

Grande and Schiwietz [65] with the UCA consider that the underestimation is due to the contribution of projectile electron capture and loss. The SLPA results displayed in Figure 7.11 are quite similar to CasP5.0[65] without loss. To this stage and related only to the SLPA calculations, we consider as first step to review the values for the excitation energy. Changes in this value affects more to outer-than to inner-shells, so the effect will be noted in the low to intermediate energy region.

In Figure 7.12 we display the SLPA results and the corresponding measured values for energy loss straggling of the four rare gases for protons. The results are good, but for Xe they seem to underestimate the experimental data. The comparison of this collective electron model with the other independent electron formalisms, such as the UCA, the CDW-EIS,[96, 97] or the continuum distorted wave (CDW)[98] methods would be a good framework for future developments. Note that the CDW[98] and CDW-EIS[96, 97] methods use the same scattering wave function for the final state in the exit channel. They differ in entrance channel, where the CDW method employs the full Coulomb wave function for the electronic continuum state, which is in the CDW-EIS method approximated by the associated asymptotic form given by the eikonal logarithmic Coulomb phase. This difference yields the corresponding difference in the perturbation potentials in the CDW and CDW-EIS methods.

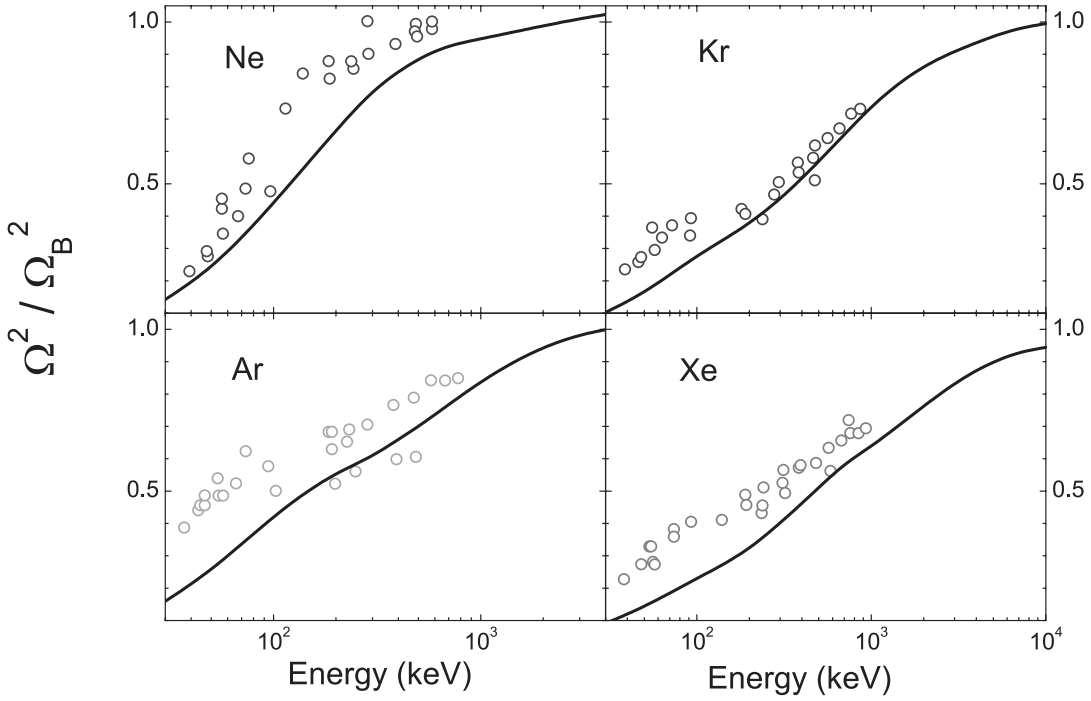

Figure 7.12 Straggling of rare gases for H^+. The curves correspond to the SLPA results. Experimental data by Besenbacher et al.[68]

The SLPA presents no specific problem to deal with the straggling and the stopping power, its calculation is straightforward. On the contrary, numerical difficulties are found to calculate the stopping power and straggling within the CDW-EIS approach. These magnitudes involve the elements, first and second moments of the energy, which depend on the behavior of very energetic electrons. The CDW-EIS approximation has serious numerical problems in two fronts. First, a good description of energetic electrons is required, which demands not only a calculation of a substantial grid of energies in this region (that would not contribute to the ionization cross section). Second, these states require a large amount of angular momenta $l_{\max}$ to describe the final continuum state.

To illustrate this point, Figure 7.13 shows the straggling and the stopping power of protons in Ne as a function of the proton velocity. Three sets of values are displayed: the results of CDW-EIS calculations with $l_{\max} = 4, 8$, and the *exact* value ($l_{\max} \approx 28$). This *exact* value agrees quite well with the SLPA, as can be observed in Figure 7.13. As the proton velocity increases, the straggling evidently requires a greater amount of angular momenta which makes the calculation more lengthy and harder. In addition, inner-shells become very important sources for the straggling. Although these inner-shells hardly contribute to the ionization cross sections, or even

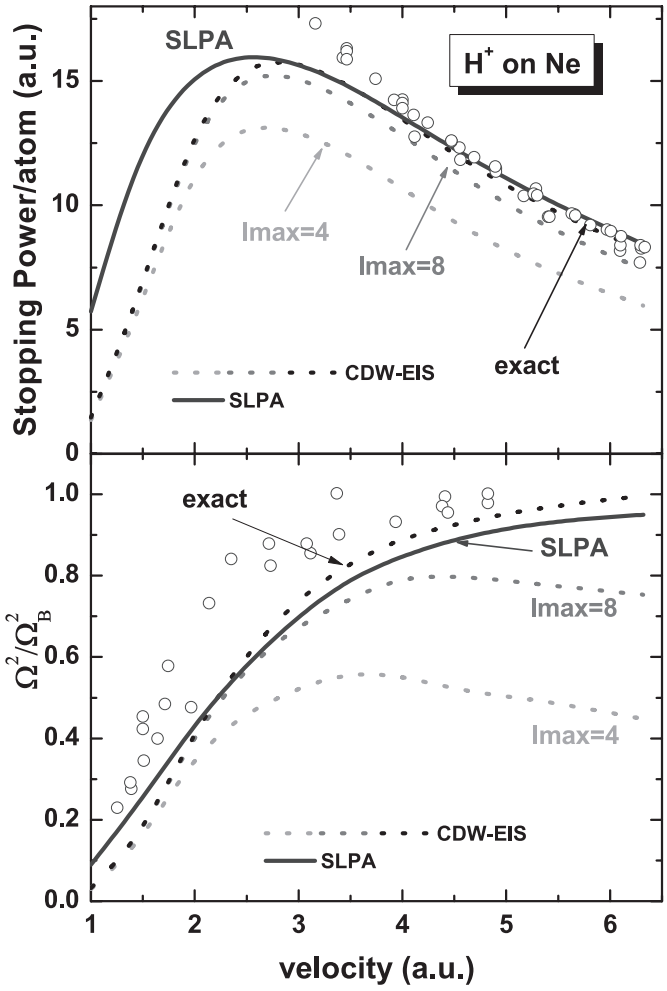

Figure 7.13 Stopping and straggling of H^+ in Ne. The curves correspond to the SLPA and CDW-EIS results, as marked in the figures. CDW-EIS values for different L_{max} are shown (see the text for details).

to the stopping power in our range of energy, they do contribute to the energy loss straggling. While the outer-shells are enough to calculate the cross section, for the straggling even deep shells are important. This makes the CDW-EIS calculation highly demanding in terms of computing time. This is a great advantage of the SLPA over distorted wave methods.

5. IONIZATION PROBABILITIES

As mentioned in the introduction, the energy moment of zero order, or cross section, is a much more sensitive parameter for the theoretical model than the stopping or straggling. In what follows we show the results of this dielectric model to deal with the description of a fundamental collisional process, the ionization.

5.1 Total ionization cross sections

The total ionization probabilities are calculated from Eq. (2) with $t = 0$. In Figure 7.14 we display the SLPA results for total ionization cross section of protons in four rare gases. We also include, as in the previous section, the comparison with the CDW-EIS values. The experimental total ionization cross sections include not only the direct ionization but also the post-collisional ionization also. As proved from multiple ionization calculations including Auger-type post-collisional contributions, the theoretical total cross section must include this contribution too.

The total cross sections displayed in Figure 7.14 are calculated adding the ionization of each sub-shell, and are afterwards corrected to include post-collisional ionization. To this end we used the ratios between total cross sections with and without post-collisional ionization in Ref. 99. In fact, this contribution is negligible for Ne and Ar targets, so the total cross sections are just the addition over the sub-shell contributions. But post-collisional influence increases with the target atomic number. For Kr it goes

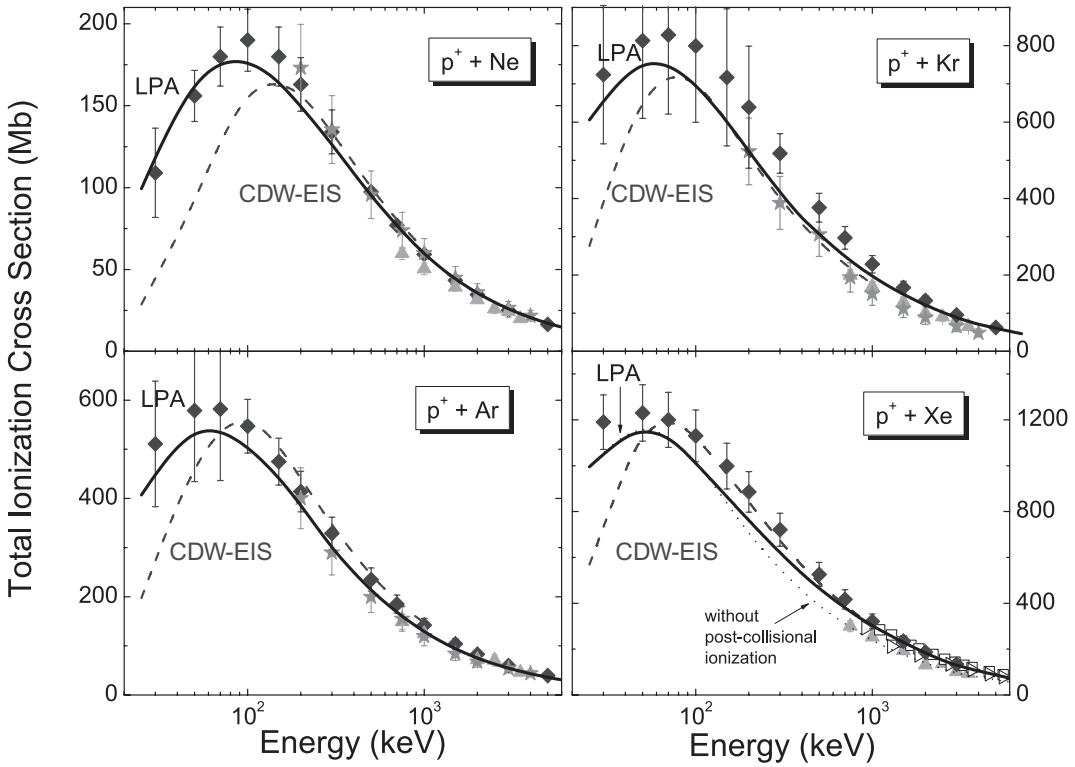

Figure 7.14 Total ionization cross sections of rare gases by proton impact. Curves: solid lines, present SLPA results; dashed lines, CDW-EIS calculations.[99] Symbols: experimental data by DuBois et al.[100] and Cavalcanti et al.[101] and recommended values by Rudd et al.[102] For Xe, we also included the electron impact data at high energies by Schram et al.[103] and by Nagy et al.[104]

from 5% at 300 keV to 24% at 5 MeV, and for Xe from 15% at 300 keV to 32% at 5 MeV (see Table 1 in Ref. 99). In Figure 7.14, for Xe target, we display both, direct ionization and total ionization including post-collisional ionization. We also include in Figure 7.14 the multiple-ionization data for electron in Xe in order to extend the description to high energies. The experimental values in Xe show the importance of post-collisional ionization in the total ionization.

The SLPA total ionization cross sections displayed in Figure 7.14 are amazing. The SLPA is good in the same energy region that the CDW-EIS. These values for ionization cross sections together with the stopping and straggling comparison in Figures 7.11 and 7.12 establish the SLPA as a good framework for further calculations.

These results consider the contribution of every shell of target electrons. We have also test the model for ionization of certain shells, such as K-shell of low Z elements[21] or, recent calculations for L- and M-shells of Au, Pb, and Bi,[8] with good agreement with the experimental data.

5.2 Multiple ionization

Multiple ionization is a quite demanding calculation for any theoretical model. It depends on the probabilities as function of the impact parameter. The SLPA implies a space-mean value of the dielectric response as given by Eq. (3). In principle the capability to describe total values may not be valid for the differential description. Moreover, the SLPA depends directly on the density of electrons of each sub-shell. It is tight to the zeros of the density distribution.

In Figure 7.15 we display the SLPA results for multiple ionization of Kr by high energy proton impact. In a many-electron description like this, the multiple ionization follows a Poisson distribution (instead of the multinomial distribution of the independent electron models).

The high energy region is governed by the post-collisional ionization.[27] The values displayed in Figure 7.15 take into account the post-collisional ionization following the method described in Ref. 27. This method includes the post-collisional electron emission in a semiempirical way by employing branching ratios of ionization distribution measured in sophisticated photo ionization experiments (see for example the values tabulated in Ref. 106).

We also display in Figure 7.15 the theoretical values for direct multiple ionization, in order to make the importance of the post-collisional

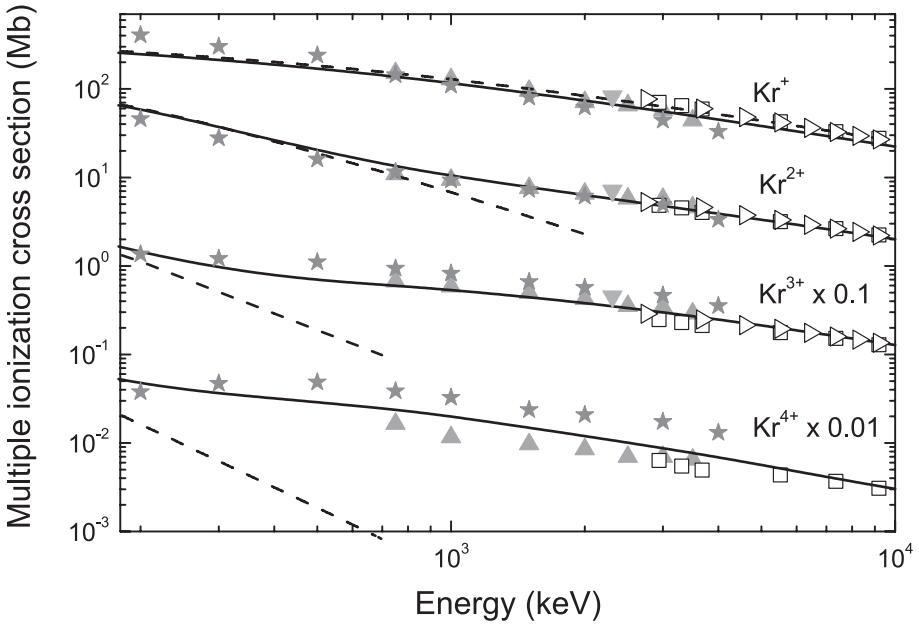

Figure 7.15 Multiple ionization of Kr by proton impact. Curves: SLPA results with (solid line) and without (dashed line) post-collisional ionization. Symbols: stars, DuBois et al.;[100] full up-triangles, Cavalcanti et al.;[101] full down-triangles, Haugen et al.;[105] open symbols for high energy electron impact data, open squares Schram et al.;[103] open triangles, Nagy et al.[104]

contribution clearer. The direct multiple ionization almost describes the single-ionization, but double-ionization cannot be explained only with direct ionization above 1 MeV. For higher orders of ionization, the importance of the post-collisional contribution increases at even lower energies than double-ionization, as can be noted for triple and quadruple ionization of Kr. As observed in Figure 7.15, the agreement of the SLPA with the experimental data is good. However some differences have been found for other targets (mainly for Ne) that require further research (analyzes of the branching ratios employed, other post-collisional contributions not considered, possibility of a semi-localized model, not so tied to the zeros of the density of electrons, etc.).

5.3 Differential cross sections

Another test for the SLPA is the differential cross section as function of the electron energy. In Figure 7.16 we display the SLPA results and compare them with experimental data by Rudd [107, 108] and by Toburen.[109] Two kinds of differential values are displayed: the differential cross sections $d\sigma/d\omega$, with ω the energy transferred to the emitted electron; and

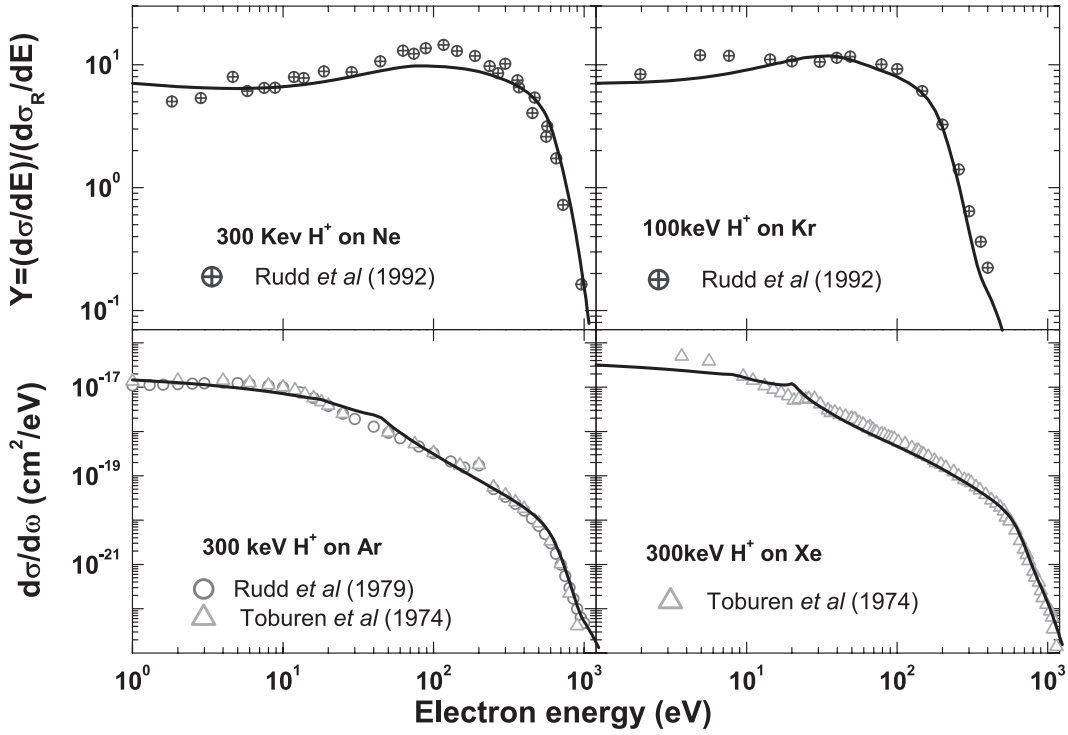

Figure 7.16 SLPA Differential ionization cross sections as function of the energy of the emitted electron for protons in Ar and Xe targets. Platzman plots for protons in Ne and Kr targets. Experimental data in Refs. 107–109.

the Platzman plots Y, which is a ratio between $\mathrm{d}\sigma/\mathrm{d}\omega$ and the modified Rutherford differential cross section $(\mathrm{d}\sigma/\mathrm{d}\omega)_{\mathrm{R}}$ by impact of one electron with the same energy,[110]

$$Y = \frac{\mathrm{d}\sigma/\mathrm{d}\omega}{(\mathrm{d}\sigma/\mathrm{d}\omega)_{\mathrm{R}}} = \frac{v^2(\omega + I)^2}{4\pi}\,\mathrm{d}\sigma/\mathrm{d}\omega, \tag{14}$$

where I is the binding energy of the outermost shell. The difference between the modified Rutherford expression and the "original" one is the presence of I. For the rare gases we used the values of Bunge et al.[40] (I=0.850, 0.591, 0.524, and 0.457 a.u. for Ne, Ar, Kr, and Xe, respectively). The energy distributions present a scale involving several orders of magnitudes and so the finer details could go unnoticed. An alternative way to plot this is the Platzman plot, whose physical interpretation is the effective number of electrons. The magnitude Y is a powerful tool for analyzing and identifying the different features in the differential cross sections in fine detail.[110]

In Figure 7.16 we present the theoretical Platzman plots for Ne and Kr, while for Ar and Xe we display the differential cross sections $d\sigma/d\omega$. The SLPA results displayed in this figure are actually overwhelming. The distribution in electron energy describes the experimental data quite well. The comparison with a much more sophisticated and computer-time consuming calculation as the CDW-EIS confirms this evaluation (see this comparison in Ref. 110).

6. CONCLUSIONS AND FUTURE PROSPECTS

In this chapter the properties, possibilities, and ranges of validity of the SLPA have been presented, analyzed, and compared with other theoretical descriptions and with experimental data. This comparison for stopping power, energy loss straggling, and ionization cross sections, establishes this model as a trustworthy alternative to the independent electron model calculations. In addition, the SLPA is a simple-low-time calculation, and allows to correctly describe the inner-shells, which proved to be very important in energy loss straggling calculations

The possibilities for further developments may start in three different areas:

i. *The extension of the model to complex targets:* As far as the space dependent density of electrons in the shell and energies are available the SLPA calculation can be performed. This seems to be the next and most important step, with a wide spectrum of possibilities to deal with molecular, clusters, or even bio-structures.

ii. *A delocalized approximation for multiple ionization:* The SLPA describes the response of the bound electrons as function of their density. In this way the SLPA cancels where the density of electrons does. But the interaction with the ion should include a region around each point. This may be taken into account through a delocalized version that does not change the total values, which is currently under study.

iii. *Antiscreening:* Finally the description of the inelastic processes of the target with a dielectric function states a difference between projectile and target. Extending the SLPA to describe inelastic processes in the projectile should not be difficult, and would allow to extend the model to deal with antiscreening processes (inelastic processes in both centers[111]).

ACKNOWLEDGMENTS

This work was partially supported by the Consejo Nacional de Investigaciones Científicas y Técnicas, and the Agencia Nacional de Promoción Científica y Tecnológica of Argentina, as well as by the University of Buenos Aires.

REFERENCES

1. Belkić, Dž.; Mančev, I.; Hanssen, J. Four-body methods for high-energy ion-atom collisions. *Rev. Mod. Phys.* **2008**, *80*, 249.
2. Belkić, Dž. *Quantum Theory of High-Energy Ion-Atom Collisions*; Taylor and Francis: London, 2008.
3. Schardt, D.; Elsasser, T.; Schuls-Ertner, D. Heavy-ion tumor therapy: physical radiobiological benefits. *Rev. Mod. Phys.* **2010**, *82*, 383.
4. Belkić, Dž. Reviews of theories on ionization in fast ion-atom collisions with prospects for applications to hadron therapy. *J. Math. Chem.* **2010**, *47*, 1366.
5. Paganatti, H. Range uncertainties in proton therapy and the role of Monte Carlo simulations. *Phys. Med. Biol.* **2012**, *57*, R99.
6. Paul, H. The Stopping Power of Matter for Positive Ions. In *Modern Practices in Radiation Therapy*; Natanasabapathi, G., Ed.; InTech, 2012; p 113. <http://www.intechopen.com/books/modern-practices-in-radiation-therapy>.
7. Montanari, C. C.; Archubi, C. D.; Mitnik, D. M., et al. Energy loss of protons in Au, Pb, and Bi using relativistic wave functions. *Phys. Rev. A* **2009**, *79*, 032903.
8. Montanari, C. C.; Mitnik, D. M.; Miraglia, J. E. A collective model for inner shell ionization of very heavy targets. *Radiat. Eff. Defects Solids* **2011**, *166*, 338.
9. Echenique, P. M.; Flores, F.; Ritchie, R. H. Dynamic screening of ions in condensed matter. *Solid State Phys.* **1990**, *43*, 229.
10. Lindhard, J. On the properties of a gas of charged particles. *Mat. Fys. Medd. Dan. Vid. Selsk* **1954**, *28*, 1.
11. Ritchie, R. H. Interaction of charged particles with a degenerate fermi-dirac electron gas. *Phys. Rev.* **1959**, *114*, 644.
12. Lindhard, J.; Scharff, M. Energy loss in matter by fast particles of low charge. *Mat. Fys. Medd. Dan. Vid. Selsk* **1953**, *27*, 1.
13. Bonderup, E. Stopping of swift protons evaluated from statistical atomic model. *Mat. Fys. Medd. Dan. Vid. Selsk* **1967**, *35*, 1.
14. Rousseau, C. C.; Chu, W. K.; Powers, D. Calculations of stopping cross sections for 0.8- to 2.0-MeV alpha particles. *Phys. Rev. A* **1971**, *4*, 1066.
15. Chu, W. K.; Powers, D. Calculations of mean excitation energy for all elements. *Rev. Lett. A* **1972**, *40*, 23.
16. Wang, Y.-N.; Ma, T.-C. Stopping power for hydrogen molecular ions in solids: influence of the inner-shell electrons of target atoms. *Phys. Rev. A* **1994**, *50*, 3192.
17. Fuhr, J. D.; Ponce, V. H.; García de Abajo, F. J., et al. Dynamic screening of fast ions moving in solids. *Phys. Rev. B* **1998**, *57*, 9329.
18. Montanari, C. C.; Miraglia, J. E.; Arista, N. R. Dynamics of solid inner-shell electrons in collisions with bare and dressed swift ions. *Phys. Rev. A* **2002**, *66*, 042902.
19. Montanari, C. C.; Miraglia, J. E.; Arista, N. R. Antiscreening mode of projectile-electron loss. *Phys. Rev. A* **2003**, *67*, 062702.
20. Kadhane, U.; Montanari, C. C.; Tribedi, L. C. K-shell processes in heavy-ion collisions in solids and the local plasma approximation. *Phys. Rev. A* **2003**, *67*, 032703.

21. Kadhane, U.; Montanari, C. C.; Tribedi, L. C. Experimental study of K-shell ionization of low-Z solids in collisions with intermediate-velocity carbon ions and the local plasma approximation. *J. Phys. B* **2003**, *36*, 3043.
22. Lantschner, G. H.; Eckardt, J. C.; Lifschitz, A. F. Energy loss of helium ions in zinc. *Phys. Rev. A* **2004**, *69*, 062903.
23. Kadhane, U.; Kumar, A.; Montanari, C. C. K-shell ionization of low Z elements in ion–solid collisions and applicability of local plasma approximation. *Radiat. Phys. Chem.* **2006**, *75*, 1542.
24. Montanari, C. C.; Miraglia, J. E. Stopping power for swift dressed ions. *Phys. Rev. A* **2006**, *73*, 024901.
25. Montanari, C. C.; Miraglia, J. E.; Heredia-Avalos, S. Calculation of energy-loss straggling of C, Al, Si, and Cu for fast H, He, and Li ions. *Phys. Rev. A* **2007**, *75*, 022903.
26. Garcia, A. J.; Miraglia, J. E. Influence of surface channeling in the stopping of protons colliding with LiF surfaces. *Phys. Rev. A* **2006**, *74*, 012902.
27. Archubi, C. D.; Montanari, C. C.; Miraglia, J. E. Many-electron model for multiple ionization in atomic collisions. *J. Phys. B: At. Mol. Opt. Phys.* **2007**, *40*, 943.
28. Miraglia, J. E.; Gravielle, M. S. Ionization of the He, Ne, Ar, Kr, and Xe isoelectronic series by proton impact. *Phys. Rev. A* **2008**, *78*, 052705.
29. Montanari, C. C.; Miraglia, J. E.; Behar, M., et al. Theoretical and experimental study of energy loss of Li ions in Zn. *Phys. Rev. A* **2008**, 77, 042901.
30. Cantero, E. D.; Fadanelli, R. C.; Montanari, C. C., et al. Experimental and theoretical study of the energy loss of Be and B ions in Zn. *Phys. Rev. A* **2009**, *79*, 042904.
31. Montanari, C. C.; Miraglia, J. E. *Theoretical Stopping Power of Copper for Protons Using the Shellwise Local Plasma Approximation*; Cornell University Library, 2009. Available from: <arXiv:0904.1386v1> [physics.atom-ph].
32. Montanari, C. C.; Mitnik, D. M.; Archubi, C. D., et al. Energy loss of protons in W using fully relativistic calculations and mean excitation energies of W, Au, Pb, and Bi. *Phys. Rev. A* **2009**, *80*, 012901.
33. Cantero, E. D.; Montanari, C. C.; Behar, M., et al. Experimental and theoretical study of the energy loss of C and O in Zn. *Phys. Rev. A* **2011**, *84*, 014902.
34. Meltzer, D. E.; Sabin, J. R.; Trickey, S. B. Calculation of mean excitation energy and stopping cross section in the orbital local plasma approximation. *Phys. Rev. A* **1990**, *41*, 220.
35. Levine, Z. H.; Louie, S. G. New model dielectric function and exchange-correlation potential for semiconductors and insulators. *Phys. Rev. B* **1982**, *25*, 6310.
36. Mermin, N. D. Lindhard dielectric function in the relaxation-time approximation. *Phys. Rev. B* **1970**, *1*, 2362.
37. Palik, E. D., Ghosh, G., editors *The Electronic Handbook of Optical Constants of Solids*; CA Academic: San Diego, 1999.
38. Isaacson, D. *Compilation of rs Values*; Radiation and Solid State Laboratory, New York University: New York, 1975; Doc. No. 02698.
39. Clementti, E.; Roetti, C. Roothaan–Hartree–Fock atomic wavefunctions: basis functions and their coefficients for ground and certain excited states of neutral and ionized atoms, Z = 54. *At. Data Nucl. Data Tables* **1974**, *14*, 177.
40. Bunge, C. F.; Barrientos, J. A.; Bunge, A.V., et al. Hartree–Fock and Roothaan–Hartree–Fock energies for the ground states of He through Xe. *Phys. Rev. A* **1992**, *46*, 3691.
41. Flannery, M. R.; Levi, H. Simple analytic expression for general two-center Coulomb integrals. *J. Chem. Phys.* **1969**, *50*, 2938.
42. Paul, H. New developments in stopping power for fast ions. *Nucl. Instrum. Methods Phys. Res. B* **2007**, *261*, 1176.

43. International Commission on Radiation Units and Measurements, ICRU Report 73, Oxford University Press, Oxford, 2005.
44. ICRU Report 49, International Commission on Radiation Units and Measurements, Bethesda, MD, 1993.
45. Paul, H. Stopping Power for Light Ions. *Graphs, Data, Comments and Programs*. <http://www.exphys.uni-linz.ac.at/stopping>.
46. Ziegler, J. F. The Stopping and Range of Ions in Matter. <http://www.srim.org>.
47. Sigmund, P. Particle Penetration and Radiation Effects Springer Series in Solid-State Physics; Springer: Berlin, 2006.
48. Arista, N. R. Energy loss of ions in solids: non-linear calculations for slow and swift ions. *Nucl. Instrum. Methods Phys. Res. B* **2002**, *195*, 91.
49. Grande, P. L.; Schiwietz, G. Ionization and Energy Loss Beyond Perturbation Theory. In , ; Cabrera-Trujillo, R., Sabin, J., Eds.; Advances in Quantum Chemistry; Elsevier: New York, 2004; 45, pp 7.
50. Abril, I.; Garcia-Molina, R.; Denton, CD., et al. Dielectric description of wakes and stopping powers in solids. *Phys Rev. A* **1998**, *58*, 357.
51. Balluc, N.; Abe, K.; Boutard, J. L., et al. Status of R&D activities on materials for fusion power reactors. *Nucl. Fusion* **2007**, *47*, S696.
52. Oreg, J.; Goldstein, W. H.; Klapisch, M., et al. Autoionization and radiationless electron capture in complex spectra. *Phys. Rev. A* **1991**, *44*, 1750.
53. Williams, G. P. *Electron Binding Energies of the Elements*; CRC Handbook of Chemistry and Physics, 66th ed.; Electron Binding Energies, X-Ray Data Booklet, Lawrence Berkeley Laboratory Pub-490 Rev., 1986; Vol. F170, Chapter 2.2. <http://www.jlab.org/gwyn/ebindene.html>
54. Arista, N. R. Charge States and Energy Loss of Ions in Solids. In *Ion Beam Science, Solved and Unsolved Problems*; Sigmund, P., Ed.; Mat. Fis. Medd. **2006**, *52*, 595.
55. Müller, J.; Bürgdorfer, J. Dynamical thresholds for the existence of excited electronic states of fast ions in solids. *Phys. Rev. A* **1991**, *43*, 6027.
56. Paul, H. Recent results in stopping power for positive ions, some critical comments. *Nucl. Instrum. Methods Phys. Res. B* **2010**, *268*, 3421.
57. Martinez-Tamayo, G.; Eckardt, J. C.; Lantschner, G. H. Energy loss of H^+ and He^+ in Al, Zn, and Au in the very low- to intermediate-energy range. *Phys. Rev. A* **1996**, *54*, 3131.
58. Heredia-Avalos, S.; Abril, I.; Denton, C. D. *J. Phys.: Condens. Matter.* **2007**, *19*, 466205.
59. Kreussler, S.; Varelas, C.; Sizmann, R. Electronic stopping power and effective charge of 50- to 230-keV D^+ and He^+ in carbon, aluminum, gold, and cesium. *Phys. Rev. B* **1982**, *26*, 6099.
60. Santry, D. C.; Werner, R. D. Stopping powers of C, Al, Si, Ti, Ni, Ag and Au for deuterons. *Nucl. Instrum. Methods Phys. Res. B* **1981**, *188*, 211.
61. Bethe, T. Zur theory des durchgangs schneller korpuskular-strahlen durch materie. *Ann. Phys.* **1930**, *5*, 325.
62. Kamakura, S.; Sakamoto, N.; Ogawa, H., et al. Mean excitation energies for the stopping power of atoms and molecules evaluated from oscillator-strength spectra. *J. Appl. Phys.* **2006**, *100*, 064905.
63. Lindhard, J.; Scharff, M. Stopping power of heavier substances. *Phys. Rev.* **1952**, *85*, 1058.
64. Schiwietz, G.; Grande, P. L. Improved charge-state formulas. *Nucl. Instrum. Methods Phys. Res. B* **2001**, *125*, 175–177.

65. Grande, P. L.; Schiwietz, G. Stopping of protons. Improved accuracy of the UCA model. *Nucl. Instrum. Methods Phys. Res. B* **2012**, *273*, 1.
66. Lifschitz, A. F.; Arista, N. R. Electronic energy loss of helium ions in aluminum using the extended-sum-rule method. *Phys. Rev. A* **1998**, *58*, 2168.
67. Arista, N. R.; Lifschitz, A. F. Non-Linear Approach to the Energy Loss of Ions in Solids. In , ; Cabrera-Trujillo, R., Sabin, J., Eds.; Advances in Quantum Chemistry; Elsevier Inc., pp 47.
68. Besenbacher, F.; Andersen, J. U.; Bonderup, E. Straggling in energy loss of energetic hydrogen and helium ions. *Nucl. Instrum. Methods Phys. Res. B* **1980**, *168*, 1.
69. Bohr, N. Penetration of atomic particles through matter. *K. Dan. Vidensk. Selsk. Mat. Fys, Medd.* **1948**, *24*, 19.
70. Ma, L.; Wang, Y.; Xue, J., et al. Energy loss and straggling of MeV ions through biological samples. *J. Appl. Phys.* **2007**, *102*, 084702.
71. Mayer, M. SIMNRA simulation program for the analysis of NRA, RBS and ERDA. *AIP Conf. Proc* **1999**, *475*, 541.
72. Heredia-Avalos, S.; Garcia-Molina, R. Energy-loss of swift $C_n^+ (n = 2 - 60)$ clusters through thin foils. *Phys. Rev. A* **2007**, *76*, 012901.
73. Garcia-Molina, R.; Abril, I.; Heredia-Avalos, S., et al. A combined molecular dynamics and Monte Carlo simulation of the spatial distribution of energy deposition by proton beams in liquid water. *Phys. Med. Biol.* **2011**, *56*, 6475.
74. Yang, Q.; O'Connor, D. J.; Wang, Z. Empirical formulae for energy loss straggling of ions in matter. *Nucl. Instrum. Methods Phys. Res. B* **1991**, *61*, 49.
75. Barradas, N. P.; Rauhala, E. Data Analysis Software for Ion Beam Analysis. In *Handbook of Modern Ion Beam Materials Analysis*, ; Wang, Y., Nastasi, M., Eds.;; MRS: Warrendale, Pennsylvania, 2009., pp 307.
76. Msimanga, M.; Pineda-Vargas, C. A. .; Comrie, C. M. Heavy ion energy loss straggling data from time of flight stopping force measurements. *Nucl. Instrum. Methods Phys. Res. B* **2012**, *273*, 6.
77. Moon, D. W.; Le, H. I.; Kim, K. J., et al. Estimation of the electronic straggling using delta-doped multilayers. *Nucl. Instrum. Methods Phys. Res. B* **2001**, *183*, 10.
78. Eckardt, J. C.; Lantschner, G. H. Determination of thin foil thickness inhomogeneities by analysis of ion beam energy loss spectra. *Thin Solid Films* **1994**, *249*, 11.
79. Hsu, J. Y.; Yu, Y. C.; Liang, J. H. et al. Energy loss of He, Li and B isotopes with MeV energies in *Au*. *Nucl. Instrum. Methods Phys. Res. B* **2004**, *219–220,* 251.
80. Kido, Y. Energy straggling for fast proton beams passing through solid materials. *Nucl. Instrum. Methods Phys. Res. B* **1987**, *347*, 24–25.
81. Kido, Y.; Koshikawa, T. Energy straggling for medium-energy H+ beams penetrating Cu, Ag, and Pt. *Phys. Rev. A* **1991**, *44*, 1759.
82. Kawano, A.; Kido, Y. Effects of energy straggling on surface analysis with fast ion beams. *J. Appl. Phys.* **1988**, *63*, 75.
83. Amadon, S.; Lanford, W. A. He stopping power and straggle in Al, Ti, Co, Cu, Ag, Ta, and Au from 1.5 to 4 MeV. *Nucl. Instrum. Methods Phys. Res. B* **2006**, *249*, 34.
84. Eckardt, J. C.; Lantschner, G. H. Experimental energy straggling of protons in thin solid foils. *Nucl. Instrum. Methods Phys. Res. B* **2001**, *93*, 175–177.
85. Alberts, H. W.; Malherbe, J. B. Energy loss and straggling of p-, d- and a-particles in Au in the energy region 0.2 to 2.4 MeV. *Radiat. Eff.* **1983**, *69*, 231.
86. Chu, W. K. Calculation of energy straggling for protons and helium ions. *Phys. Rev. A* **1976**, *13*, 2057.
87. Hoffman, G. E.; Powers, D. Energy straggling of a particles in solid materials. *Phys. Rev. A* **1976**, *13*, 2042.

88. Friedland, E.; Kotze, C. P. Energy-loss straggling of protons, deuterons and a-particles in copper. *Nucl. Instrum. Methods Phys. Res.* **1981**, *191*, 490.
89. Livingston, M. S.; Bethe, H. A. Nuclear dynamics, experimental. *Rev. Mod. Phys.* **1937**, *9*, 245.
90. Sigmund, P.; Schinner, A. Barkas effect, shell correction, screening and correlation in collisional energy-loss straggling of an ion beam. *Eur. Phys. J. D* **2003**, *23*, 201.
91. Andersen, H. H.; Csete, A.; Ichioka, T., et al. An apparatus to measure stopping powers for low-energy antiprotons and protons. *Nucl. Instrum. Methods Phys. Res. B* **2002**, *194*, 217.
92. Møller, S. P.; Csete, A.; Ichioka, T., et al. Antiproton and proton energy loss straggling at keV energies. *Eur. Phys. J. D* **2008**, *46*, 89.
93. Andersen, H. H.; Besenbacher, F.; Goddiksen, P. Stopping power and straggling of 80–500 keV lithium ions in C, Al, Ni, Cu, Se, Ag, and Te. *Nucl. Instrum. Methods Phys. Res.* **1980**, *168*, 75.
94. Eckardt, J. C. Energy loss and straggling of protons and helium ions traversing some thin solid foils. *Phys. Rev. A* **1978**, *18*, 426.
95. Malherbe, J. B.; Alberts, H. W. Energy-loss straggling in lead of p, d and a-particles in the energy region 0.2–2.5 MeV. *Nucl. Instrum. Methods Phys. Res. B* **1982**, *196*, 499.
96. Crothers, D. S. F.; McCann, J. F. *J. Phys. B: At. Mol. Opt. Phys.* **1983**, *16*, 3229.
97. Fainstein, P. D.; Ponce, V. H.; Rivarola, R. D. A theoretical model for ionisation in ion-atom collisions. Application for the impact of multicharged projectiles on helium. *J. Phys. B: At. Mol. Opt. Phys.* **1988**, *21*, 287.
98. Belkić, Dž. A quantum theory of ionization in fast collisions between ions and atomic systems. *J. Phys. B* **1978**, *20*, 3529.
99. Montanari, C. C.; Miraglia, J. E. Antiproton, proton and electron impact multiple ionization of rare gases. *J. Phys. B: At. Mol. Opt. Phys.* **2012**, *45*, 105201.
100. DuBois, R. D.; Toburen, L. H.; Rudd, M. E. Multiple ionization of rare gases by H^+ and He^+ impact. *Phys. Rev. A* **1984**, *29*, 70.
101. Cavalcanti, E. G.; Sigaud, G. M.; Montenegro, E. C. Absolute cross sections for multiple ionization of noble gases by swift proton impact. *J. Phys. B: At. Mol. Opt. Phys.* **2003**, *36*, 3087.
102. Rudd, M. E.; Kim, Y-K.; Madison, D. H.; Gallagher, J. W. Electron production in proton collisions: total cross sections. *Rev. Mod. Phys.* **1985**, *57*, 965.
103. Schram, B. L.; Boerboom, A. J. H.; Kistermaker, J. Partial ionization cross sections of noble gases for electrons with energy 0.5–16 keV: I. Helium and neon. *Physica* **1966**, *32*, 185.Schram, B. L. Partial ionization cross sections of noble gases for electrons with energy 0.5–18 keV: II. Argon, Krypton and Xenon. *Physica* **1966**, *32*, 197.
104. Nagy, P.; Skutlartz, A.; Schmidt, V., et al. Absolute ionisation cross sections for electron impact in rare gases. *J. Phys. B: At. Mol. Opt. Phys.* **1980**, *13*, 1249.
105. Haugen, H. K.; Andersen, L. H.; Hvelplund, P., et al. Multiple ionization of noble gases by fully stripped ions. *Phys. Rev. A* **1982**, *26*, 1962.
106. Montanari, C. C.; Montenegro, E. C.; Miraglia, J. E. CDW-EIS calculations for multiple ionization of Ne, Ar, Kr and Xe by the impact of H^+ and He^+, including post-collisional electron emission. *J. Phys. B: At. Mol. Opt. Phys.* **2010**, *43*, 165201.
107. Rudd, M. E.; Kim, Y.-K.; Madison, D. H., et al. Electron production in proton collisions with atoms and molecules: energy distributions. *Rev. Mod. Phys.* **1992**, *64*, 441.
108. Rudd, M. E.; Toburen, L. H.; Stolterfoht, N. Differential cross sections for ejection of electrons from argon by protons. *At. Data Nucl. Data Tables* **1979**, *23*, 405.

109. Toburen, L. H. Distribution in energy and angle of electrons ejected from xenon by 0.3- to 2.0-MeV protons. *Phys. Rev. A* **1974**, *9*, 2505.
110. Miraglia, J. E. Ionization of He, Ne, Ar, Kr, and Xe by proton impact: single differential distributions in energy and angles. *Phys. Rev. A* **2009**, *79*, 022708.
111. Montenegro, E. C.; Meyerhof, W. E. Sum rules and electron–electron interaction in two-center scattering. *Phys. Rev. A* **1991**, *43*, 2289.